1-27-2022

Understanding the Relationship between Genetic Markers and Skeletal Remains: Implications for Forensic Anthropology and Phenotype-Genotype Studies

Kamar Afra
University of Tennessee, Knoxville

Bridget F.B. Algee-Hewitt
Stanford University

Michelle D. Hamilton
Texas State University - San Marcos

Understanding the Relationship between Genetic Markers and Skeletal Remains: Implications for Forensic Anthropology and Phenotype-Genotype Studies

Kamar Afra,[1]* Bridget F. B. Algee-Hewitt,[2] and Michelle D. Hamilton[3]

[1]Department of Anthropology, University of Tennessee, Knoxville, Tennessee, USA.

[2]Humanities and Sciences Interdepartmental Programs, Stanford University, Stanford, California, USA.

[3]Department of Anthropology, Texas State University, San Marcos, Texas, USA.

*Correspondence to: Kamar Afra, University of Tennessee, Department of Anthropology, 502 Strong Hall, 1621 Cumberland Avenue, Knoxville, TN 37996 USA. E-mail: kamar.afra@gmail.com.

Short Title: Assessment of Correlation between Phenotype and Genotype

KEY WORDS: PHENOTYPE-GENOTYPE ASSESSMENT, FORENSIC ANTHROPOLOGY, HUMAN IDENTIFICATION, FORENSIC FACIAL RECONSTRUCTION, CRANIOMETRICS, SINGLE-NUCLEOTIDE POLYMORPHISMS (SNPS).

Abstract

Human identification techniques have been a leading tool to hold perpetrators accountable, give families closure, and reconstruct faces on skulls. This project is a pilot study to critically examine three disciplines that fall under the human identification umbrella: forensic anthropology, forensic genetics, and forensic art. Current facial research in genetics focuses on data from living individuals where specific single-nucleotide polymorphisms (SNPs) that influence specific regions of the face have been found. This study asses the translation of these same regions to craniometric dimensions (inter-landmark distances) of the underlying skull itself. The goal of this project is to provide information regarding the correlation of craniometric measurements and SNPs, as well as encourage interdisciplinary work within the forensic sciences. We examined a selection of candidate SNPs currently identified in the literature to determine if there were correlations between inter-landmark distances and those SNPs within the same individual. A series of 98 craniometric landmarks were collected from 17 documented skulls from the Texas State Donated Skeletal Collection using a 3D Microscribe digitizer. Criteria for inclusion in this study included European American ancestry, the presence of intact skulls, and presence of associated donor blood cards collected at the time of body donation. Using these blood samples, DNA from each individual was extracted, amplified, and sequenced through Next Generation Sequencing for the specific chosen SNPs. Afterward, bioinformatics tests were applied to observe the presence or absence of the major or minor alleles in the specific locations on the genome. After determining the presence or absence of an SNP (minor allele), a set of statistical tests were performed including: Spearman's correlation between the craniometric measurements and the individual's genetic data variables; two-way hierarchical clustering and Bootstrap Forest modelling between variables that demonstrated significant correlation; a principal component analysis was performed on the craniometric data (inter-

landmark measurements) and genetic data (SNP presence/absence) in order to check the homogeneity of each data set; and finally, a pair-wise Procrustes analysis was completed on the correlation of the two data sets as different groups. The results indicate a correlation in various degrees between the targeted craniofacial regions and the targeted SNPs. There were 11 SNPs that showed significant correlation ($p < 0.05$). However, the correlations were not as expected and showed some interesting results. By group level there was no significant correlation, however, there was correlation at the individual level. While some SNPs affected the soft tissues only, others showed correlations with the skull (hard tissue), a finding that had not been previously known. By combining craniometric and DNA analyses to leverage genotype-phenotype associations, there is great potential to expand the discourse of current facial approximation and to, thereby, provide new investigative tools for human identification in forensic anthropology.

Efforts to improve human identification, especially in the context of skeletonized or badly decomposed remains, have benefited from rapid evolution in the forensic sciences. New methodologies are diversifying the ways forensic anthropologists estimate the components of the biological profile or elicit supporting information from the skeleton that may help to produce investigative leads. New technologies for DNA analysis have enriched all areas of work – from isolation to K-Q matching – and have generated new opportunities for accessing information on the unknown individual that was once only available in life or when using optimal samples, and certainly not from damaged, fragmented bones that were presumed to yield only highly degraded DNA. The combination of genetics and forensic anthropology has changed the landscape of human identification by expanding the ranges of techniques, filling knowledge gaps, and strengthening evidence. Nevertheless, there are casework challenges and scientific limitations that can impede case evaluation and an assistive or positive identification: samples can be too compromised for reliable metric or DNA assessment, reference data may be missing at the level of the population for comparative analyses, antemortem, dental, or imaging records may not be available for matching, or there may be no data on close relatives with which to make a kin-based identification. In such instances, when both forensic anthropology and genetics fail to produce evidence in support of identity, law enforcement agencies may turn to other investigative options, including forensic art; specifically, facial approximation via 2D and 3D reconstruction. While forensic artists draw upon a mix of anatomical and anthropometric information (Gerasimov 1971; Wilkinson 2004), sourcing, for example, tissue depth markers and morphological landmarks and measurements (Taylor 2001), forensic reconstructions are deeply rooted in experiential knowledge and often rely upon subjective artistic interpretation to finalize the reconstruction. There is a need to not only reevaluate current facial reconstruction procedures but to rethink the approach: with the emergence of DNA-based prediction of externally visible

features at both the research and commercial levels (Budowle and van Daal 2008; NanoLabs 2016), there is the potential for great improvement with the introduction of genetics, shifting the DNA use-case from predicting facial morphology of the living in criminal justice contexts to identifying the dead for social justice in forensic anthropological casework.

Current constraints upon developing this line of research include especially the fact that studies of the human face via genetic information tends to only examine soft tissue data from living individuals (Liu et al. 2009; Peng et al. 2013; Adhikari et al. 2016; Shaffer et al. 2016; Cha et al. 2018). This focus is problematic as soft tissue is known to be affected by unique sets of variables that differ from those influencing the craniofacial skeleton (Paternoster et al. 2012; Claes et al. 2018). Further, while the cranium plays a key role in the shape of the face, very few genetic researchers have addressed the influence of the skull on the face (Maroñas et al. 2015). Absent is the link between these two kinds of data (soft tissue and skeletal) and their genetic underpinnings. Importantly, there is no research, to our knowledge, that has adequately resolved the research question that we investigate in this study: for the craniofacial complex, are the single nucleotide polymorphism (SNP) markers associated with soft tissue traits also associated with the craniofacial skeleton and thus with skeletal measurements?

For this study, we leveraged published research in genome wide association (GWAS) linking genotypic expression to soft tissue features of the face (i.e., Liu et al. 2012; Paternoster et al. 2012; Adhikari et al. 2016; Shaffer et al. 2016; Claes et al. 2018), in order to design a framework under which we could test whether there is a link between the genetic markers with facial soft-tissue associations and phenotypic expression of the skull. We generated DNA (SNP) profiles, collected cranial landmarks, and calculated standard inter-landmark distance measurements, producing a morpho-genetic dataset which we analyzed for any genotype to skeletal phenotype associations. The work presented here represents the first step of analysis in

support of a larger project investigating the role of the skull on the shape of the soft tissues of the face.

Genomic Approaches to Facial Characteristics

Early genotype-phenotype studies in developmental biology on humans tracked the expression of mutations in the genome that lead to diseases or abnormalities (Buschang and Hinton 2005; Reijnders et al. 2018; Schoenwolf et al. 2015). After the Human Genome Project was completed (Deloukas et al. 1998; Hudson et al. 1995; Stewart et al. 1997), researchers started observing the effects of genetic variation on the phenotypic expression of diseases or congenital conditions. Some of the conditions were related to the face, including cleft lip or palate that can be surgically corrected if discovered early (in utero), or during childhood (Kapp-Simon et al. 1992). Researchers were able to study and track these inherited craniofacial mutations by testing both the parents and their children (Mossey et al. 1998). This early research was not limited to medical and surgical applications. Forensic science utilized several genetic techniques for identification beginning with historic blood type determination to restriction fragment length polymorphism (RFLP), STR analysis, and next-generation sequencing (Alvarez-Cubero et al. 2017). The advancement in forensic genetics led to an interdisciplinary approach linking facial characteristics to genetic data (Little et al. 2006). The research focused on externally visible characteristics (EVCs) (Fortes et al. 2013), where researchers tried to identify genes responsible for specific phenotypic markers on the face (Shaffer et al. 2016), as well as direct phenotypic traits such as eye color and hair color (Liu et al. 2009; Walsh et al. 2012, Chaitanya et al. 2018), and integrating skin color to use for various forensic applications (Maroñas et al. 2015; Walsh et al. 2014). This new approach emerged around the world (Cho et al. 2009; Bonfante et al. 2021) to tackle the subject of facial reconstruction through genetic information and soft tissue data but

it was not confined solely to scientific research studying the intersection of orofacial clefts and facial variation (Indencleef et al. 2021) but also extended to commercial levels such as HIrisPlex-S, SHEP, ForenSeq™, IDentify, and Parabon™ Snapshot™ (Schneider et al. 2019). But, detecting different genes that may influence phenotypic expression is not without its challenges. Several researchers had attempted to identify gene expression for the phenotype using soft tissue facial measurements within different populations, acknowledging the importance of population variation (e.g., Peng et al. 2013; Adhikari et al. 2016; and Cha et al. 2018). In each of these populations, most of the identified genes were different from those in other populations, suggesting that population is an important factor. Further, as we know, gene expression is a complex process driven by many variables, both intrinsic and extrinsic, and therefore the exact genotypic-phenotypic relationships and how they are influenced by external environmental factors are often unknown (Claes et al. 2014; Hallgrímsson et. al 2007; Young et al. 2014).

Facial Artistic Approaches to Facial Characteristics

In criminal casework, when positive identifications on unidentified remains are not forthcoming, occasionally more subjective approaches such as facial reconstruction are implemented to recreate the face of an unidentified skull. Forensic facial reconstruction is an approach adopted in identification efforts and criminal proceedings. It is part of the image identification category of forensic art (Taylor 2001). Each human face is unique, even between identical twins where epigenetics can play a role in the plasticity of the face (Wilkinson 2004). There are several techniques that artists and anthropologists have developed throughout the years related to facial reconstruction: 2D facial superimposition, and 3D manual and computerized facial reconstruction (Gupta et al. 2015). Researchers have tried to develop new techniques to obtain

more objective facial reconstruction approaches, such as CT scan superimposition (Sakuma et al. 2010; Guyomarc'h et al. 2014) and 3D laser technology (Sholts et al. 2010). While 3D facial reconstruction approaches work with cranial landmarks, landmarks are standardized to each population, e.g., French populations (Guyomarc'h et al. 2014) and Korean populations (Lee et al. 2015), and this research is focused mainly on soft tissue. With the arrival of new genetic technologies and advances in SNP typing potential, DNA-driven facial reconstruction forms are currently being developed and marketed commercially for law enforcement use for forensic identification purposes. For example, after collecting genetic data using the Parabon's Snapshot DNA phenotyping system, the Parabon NanoLabs company employs machine learning (ML) to create models from genetic data to generate face templates (Steve Armentrout, personal communication, 2018), after which a Parabon forensic artist helps craft the final version for law enforcement to use (Budowle and van Daal 2008; NanoLabs 2016). Given the commercial motivation of this work, it is critical to continue to foreground research by studying the effects of different genetic variants on the face and evaluating the current facial approximation methodologies.

Materials

Sample Selection

We selected 17 skeletonized individuals, 10 males and 7 females of self-reported European American identity with intact crania and matching DNA blood cards, from the Texas State Donated Skeletal Collection at Texas State University, San Marcos. The individuals chosen for the project were required to meet four main criteria, based on the parameters defining the previously identified SNPs in the literature and practical data considerations: 1) European American population affinity. Drawing upon prior findings of a non-trivial correlation between

race and ancestry in the European American population from both cranial and DNA based analysis (Algee-Hewitt 2016; Bryc et al. 2015; Lao et al. 2014), White identity was used as a proxy for European American ancestry. This identifier was self-reported by the donors or their kin and was retrieved from the donation forms. Eligible donors needed to select White in the race section of the body donation form. 2) They were adults aged between 25 and 60 years. 3) No history of fractures, trauma, or congenital disorders affecting the face. 4) Not edentulous.

Skeletal Preparation and Data Collection

We articulated the cranium with the mandible using super glue in a method applied by forensic artists for sample preparations in forensic facial reconstruction methods (Taylor 2001). We collected a set of standard landmarks (type I, II, and III) (Bookstein 1997) and non-standard landmarks (symmetrical points to pre-existing landmarks) and semi-landmarks to capture cranial shape and calculated the inter-landmark distances (ILDs) common to forensic anthropological casework. The set of landmarks used was modified from the original 3Skull program template (Ousley 2004), which was adopted from Howells (Howells 1973). Our revised version contains 99 landmarks, as shown in Figure 1, and Table 1. In addition to these landmarks, we included two major curves, frontal and nasal, represented by a series of semi-landmarks positioned 0.5 cm apart. The coordinate data was obtained with a Microscribe digitizer via the 3Skull interface.

DNA Preparation and Analysis

All genetic sequencing work was performed at the Kang Laboratory at Texas State University. We completed a phenol-chloroform extraction with a silica-based purification using a protocol adapted from SOP-FS12014, the protocol developed by the molecular genetic laboratory at the American University of Science and Technology (AUST), Beirut, Lebanon, and other resources

(Healthcare 2010). We tested the extracted DNA for purity and quantity with the Thermo Scientific™ NanoDrop ND-1000 (Desjardins and Conklin 2010).

We targeted 20 SNPs of interest (Table 1), for which we designed our own primers using the Primer3Plus software (Untergasser et al. 2012) and sourced data from the National Center for Biotechnology Information (NCBI) database and the Genome-Wide Association Study (GWAS) database to build the genetic library. To decrease the cost of the research, we applied a multiplex approach through a dual indexed paired-end library. After the DNA extraction, two polymerase chain reactions (PCR) were completed, the first after adding the Illumina sequencing adapter, and the second after adding the sample-specific barcodes. We used the Invitrogen DNA PureLink quick gel extraction kit to isolate the DNA fragment including the amplicon, adapter, and barcode segments after each amplification. Samples were quantified first with the Qubit® 3.0 Fluorometer using the Qubit® dsDNA HS Assay Kit protocol for quality assurance, and second by quantification via qPCR according to the KAPA Library Quantification Kit Illumina®-KR0405 – v8.17 using an in-house reference library and a series of dilution to reach the optimum concentration. Once the samples were ready for sequencing with a concentration of 6 pM, we run the samples through the MiSeq Reagent Nano Kit v2 (300-cycles).

The FASTQ reads generated by MiSeq Illumina sequencer were assessed through FASTQC for quality. We used Jupyter (Toomey 2016), an IPython notebook, along with MobaXterm, a user interface for remote computing by Mobatek® to process command lines for further analysis. We used the "cutadapt" function in python (Martin 2011) to remove the adapter sequences, retaining the amplicons for 20 pre-identified SNPs. We aligned each single-ended file using a reference index adopted from H. sapiens GRCh38 found at UCSC Genome browser (Kuhn et al. 2013), then merged them together as double-ended files through a pair-end alignment with Bowtie2 (Langmead and Salzberg 2012) for each SNP of each sample using

different loops in python (McKinney 2018). The data obtained was processed through Samtools (Li H 2011) and SNP calling was completed using Bcftools (Liu et al. 2013). Finally, we obtained the targeted SNPs from the known location in each amplicon via Unix commands and AWK (Dougherty and Robbins 1997). We generated a matrix containing binary data (0 and 1) on the presence or absence of the minor allele for each sample for downstream analysis.

Statistical Methods

Combining ILDs and SNPs into Functional Groups

We paired the SNPs and ILDs according to their functional groups. We found that the different functional groups with their associated single nucleotide polymorphisms (SNP) have different landmarks related to them, and each SNP had their own set of inter-landmark distances (ILDs) that represents the associated phenotype area/functional group of the face. Figure 2 visualizes the SNP-ILD-functional group relationships, and more details are given in Supplementary Materials Table 1.

Statistical Analyses

Data were analyzed with JMP (Sall et al. 2012) and using custom R scripts (R Core Team, 2016) written by Algee-Hewitt. We used Spearman's rank-order correlation to test for associations between all the SNPs and ILDs, using the continuous data obtained from the calculated ILDs and the binary (present/absent) data obtained from SNPs. These results were explored with a two-way hierarchical clustering in order to visualize any direct relatedness or similarity between the different variables that were shown as significant previously (Phipps and Larry 1996). We also implemented a Bootstrap Forest model to resample our samples and create 100 decisions trees to generate a simulated set of predictive data. We evaluated our results with a prediction profiler

(assessment model), which provides the probability in which a certain value of the variables has an effect on predicting the values of the response. Principal component analysis (PCA) was performed for both SNPs and ILDs separately to visualize variation in space. We also executed a Procrustes analysis for the pair-wise comparison between SNPs and ILDs.

Results

Frontal Arc

The raw 3D semi-landmark data were analyzed with MorphoJ (Klingenberg 2011). The first two Principal Components (PCs) represent around 60% of the variation (Table 2 in supplementary materials).

The plot of those two PCs generated (Figure 3), in which the individuals are separated according to sex (red dot=female, blue dot=male), reveals patterns concordant with the results from PCA of the landmarks. The distribution of variation within females, between around -0.04 and 0, was smaller than the variation within males, between -0.04 and 0.06 in PC1. The Procrustes coordinates were split and plotted according to sex. The different shapes, especially around the last 10 semi-landmarks, are different between sexes. This morphology coincides with the presence of the glabella projection on the frontal bone. The low sum of squares value (0.03) for all the samples shows the small distance needed to superimpose the different shapes of the frontal arcs.

DNA Data

The alleles were differentiated according to their haplotype, and the presence of the minor alleles was coded as 1 and the absence of this allele was coded as 0, as shown in Table 2. SNPs rs2977562, rs72691108, and rs9995821 were found to have the highest presence within the

sample with 10, 9, and 8 occurrences, respectively. However, there was no presence of the following SNPs: rs10862567, rs7559271, rs3827760, rs6740960, rs17447439, rs6555969, rs5880172, rs17640804, rs10238953.

Genotypes-Phenotypes

The Spearman's correlation analysis on both the SNP and ILD data sets showed different patterns, as represented by the heat map (Figure 4). We evaluated only the most relevant out of this large pool, selecting significant correlations with p-values lower than 0.05 (Table 3). The blue spectrum shows the correlation coefficient (rho), and the pink spectrum indicates the p-value for each correlation. The absolute correlation coefficient ranged between 0.65 and 0.48. The distribution of rho values is shown with the corresponding ILDs in Figure 5. The different sizes correspond to the actual numerical value of the ILDs. There are very strong positive correlations with a p-value of 0.0076 and a rho value of 0.6228 between Ans-prosH (Anterior Nasion spine and prosthion-Howells), and Ans-prosM (Anterior Nasion spine and prosthion-Martin) and SNP rs46483792. This correlation is also shown between ILDs and SNPs from a different but related functional group: Nasal Ala length and philtrum length.

Strong negative correlation (p-value=0.0048; rho=-0.6495) was found between zygr-nas (zygion-R and nasion) and SNP rs72691108. Those two elements are also from different groups: zygion-nasion-zygion and eye-nasion-eye respectively. Another significant positive correlation between two different SNPs (rs1716852 and rs9278332) which are related to two different functional groups: cranial width and nose wing breadth, respectively.

Figure 6 shows a principal component analysis demonstrating the distribution of the statistically significant ILDs with the first two principal components representing jointly 50% of the variation. The variation of the data is presented in 16 dimensions, and an adequate

representation can be achieved by the first five principal components with 76.825% cumulative percentage.

We performed the two-way hierarchical clustering of the significant SNPs and ILDs against the clustering among the donated individuals used in this study and produced a dendrogram (Figure 7). The values computed are given in the plot shows the proximity and remoteness of the correlations in reference to the samples' distribution.

We performed a Bootstrap Forest regression model to determine if or how those ILD-SNP correlations could be useful for future predictions. In Table 4, the yellow coloration spectrum shows the different values of R-square and the pink show the mean square error. The values range between 0.35 for rs8007643 and 0.63 for rs9995821. The ones closest to rs9995821 show the highest likelihood. The lowest Root-Mean-Square Error (RMSE) is 0.23 and it is related to rs927833. The R-square range is between 0 and 1. The model represents a better fit if the R-square value is closer to 1 and the RMSE is a low value with no outliers. In these different models, the RMSE does not exceed 0.34 which presents an error of less than 3.4% across all models.

Evaluation of the random forest model was performed by producing an assessment profile of the SNP according to a certain value of the associated variable corresponding to it (as shown in Table 5). For example, if the following inter-landmark distances have these values: anterior nasal spine- subspinale (ans-ssp) 6.9281 mm, gnathion-chin protrusion point (gniipt-chpp) 13.3347 mm, most inferior nasal border R-subspinale (nlhir-ssp) 11.332 mm, subspinale-anterior nasal spine (ssp-ans) 6.9281 mm, and TMF lingual point R-pogonion (tmflptr-malapt) 28.4267mm, then the SNP rs6129564 is not present and thus the major allele is present which means that this individual has the common allele in this position. These data are interpreted in more depth in the discussion section.

Procrustes analysis was completed for all individuals with a non-random significance between SNPs and ILDs. The sum of squares obtained was 0.95 with a symmetric correlation in a symmetric Procrustes analysis with no significance, giving a p-value of 0.759. The high value of the sum of squares suggests that the data points are highly dispersed from the mean as shown in Table 6. They show no correlation and no significance.

Discussion

Analysis of SNPs and Craniometric Markers Separately

The different analyses performed on each variable group through principal components analysis (PCA) helped to clarify the nature of the variation for the sampled individuals. The PCA performed in MorphoJ for the coordinates of the 99 landmarks showed both a strong agreement among the shapes of the skulls regardless of their size, overlapping of samples regardless of sex. This suggests that for the purposes of this experiment, sex was not a determining factor in examining bilateral correlations. However, the PCA performed on the semi-landmarks obtained for the frontal arc gave different shapes by sex, especially toward the superciliary arch and the supraorbital margin of the frontal bone where the glabella and supraglabella landmarks are present (White et al. 2012). This morphology is consistent with macroscopic observations that drive cranial sex scoring approaches and reflects an area important to estimating the sex of the individual in discriminant functional analysis (Walker 2008). These findings might also be due to the older ages of the females used in this sample who ranged from 42- 58, as aging may potentially affect the robusticity of the skull (Urban et al. 2016), in turn affecting the prominence of the supraorbital margin. However, the small variation of the distance of rotations (0.03) in Figure 8 are an indication of the homogeneity of the individuals within the sample. This can be

attributed to the absence of the influence of size on the craniofacial shape in individuals from the same group (Kimmerle et al. 2008).

At the same time, there was a distinct pattern with the results of the DNA sequencing. The bioinformatics analysis showed a distinct pattern between the presence and absence of minor alleles representing the different SNPs. The 20 SNP targets chosen at the beginning of this research (culled from previous literature on soft tissue facial shapes, e.g., Adhikari et al. 2016; Claes et al. 2018; Shaffer et al. 2016) showed significance in the whole genome wide association studies. However, the individuals from this study did not have the minor alleles representing 9 out of the 20 studied SNPs. This absence may indicate that portability of results from population-level studies - such as whole genome association studies - can be variable in their application on smaller sample sizes and at the level of the individual. We chose to include four different SNPs that were found to be of significance in Latin American populations (Adhikari et al. 2016), with the expectation that they would not be significant in the European American sample. In an interesting outcome, however, the four Latin American SNPs (rs7559271, rs3827760, rs17640804, rs927833) were all absent in the samples with the exception of rs927833, as shown in Table 3. This means that while three out of the four SNPs were not present, rs927833 was present in two individuals. One of those two individuals was self-identified as “white”, but they may hold Native American ancestry according to their donation paperwork. The other individual did not have any information in their paperwork indicating a different identity. The assortment of the expressed SNPs in this study can be explained by biodistances between populations and show how geography and population history can be a factor affecting the similarities between genetic markers found among populations (Relethford 2016).

Associations between SNPs and ILDs

The results obtained from the different tests to assess the association between the genetic markers and the craniofacial measurements showed similarities, but also differences. The Spearman's rank-order correlation was a tool that helped decrease the pool for analysis by evaluating only the significant correlation between the categorial genetic input and the continuous craniometric data We only interpreted correlations with a p-value lower than 0.01. The correlation between groups on the individual level gave interesting results where there were associations that were not accounted for in previous genomic literature. These include the significant association between rs6129564 and anterior nasal spine- subspinale (ans-ssp), gnathion- chin protrusion (gniipt-chpp), most inferior nasal border R- subspinale (nlhir-ssp), and TMF lingual point R- pogonion (tmflptr-malapt). In the literature, rs6129564 is correlated with cranial width (Shaffer et al. 2016). In our hypothesis, we assigned two different measurements to this category: stephanion L- stephanion R (stpl-stpr) and Maximum frontal point L- Maximum frontal point R (xfbl-xfbr). However, the results showed that this genetic marker does not affect any of the suggested measurements, but it is associated with measurements from different functional groups related to the philtrum, chin protrusion, and nose tip. This alternative association can be an indication of underlying association related to the formation of the visceral portion of the cranium. The development of the human face occurs during week 4 to 7 of the prenatal development. During the 5th and 6th week, the frontonasal process, philtrum, and lateral and medial nasal process (nasal capsule) develop (Chiego 2019; Lieberman 2011). The visceral branchial components including Meckel’s cartilage give rise to several skeletal elements such as the petrous portion of the temporal bone and the mandible (Retzlaff 1987). This association in development occurs during a period in which environmental factors can affect the development of the embryo, especially during the 5th week. The observations of developmental timing of the cranium may explain the effects on the manifestation of genetic markers and rs6129564, for

example. This said, several factors likely affect the expression of certain markers: these can be related to environment but also to genetic inheritance, linking back to population lineage (European American in this case) (Cole et al. 2017). Together, they represent a form of gene–environment interaction.

Another unique example in those correlations is the association between rs1716852, rs9278332, and most inferior nasal border L – anterior nasal spine (nlhil-ans). In this special case, the two SNPs and the one ILD are interchangeably correlated with each other. This shows that SNPs need not be expected to have only significant correlations with an ILD, but that they can also have correlations between each other. The association between the SNPs, as genetic mutations, can be interpreted as genomic imprinting where the presence of a genetic marker can either silence or enhance the effect of another marker (Bajrami and Spiroski 2016). Thus, observing a form of gene-gene interaction.

The different significant associations between craniometric and genetic markers had also distinct results in the two-way hierarchical clustering. This test showed how the measurements that are morphologically next to each other are clustered next to each other, such as gnispt-malapt (infradentale-pogonion) and gnispt-gniipt (infradentale-gnathion). This is an interesting cluster where those landmarks lay on the midline of the face (Langley et al. 2016). But, there are several variables that do not have this association. This variation in clusters can be related to the variability of certain measurements between individuals of this sample.

Another cluster between two neighbors rs1982862 and alarl-ans (nasal ala breadth L side-anterior nasal spine) is also correlated according to functional group. Both of these variables are related to the same morphological group nasal ala length (L &R). The correlation, however, between those two variables does not match with the insignificant results obtained from Spearman's correlation where the coefficient correlation is 0.45 and the p-value is 0.072 shown

in Appendix IV. This closeness between those two variables indicates that there is an overlying relationship between them. Three different genomic researcher groups were able to find a soft tissue correlation between rs1982862 and pronasale to L- alare area (Claes et al. 2018; Paternoster et al. 2012; Shaffer et al. 2016). This association corresponds with the random clustered created between the SNP and nasal ala breadth L side- anterior nasal spine distance. However, due to the lack of any significant correlation in the non-parametric test, the association may be related to soft-tissue development that was observed in previous literature but not related directly to hard tissue.

The clustering of individuals in the two-way hierarchical analysis corresponds with the distribution of the samples in the PCA of the significant ILDs. Here, the least variable samples are clustered neighboring each other. These results confirm the notion of homogeneity of the individuals within the present sample creating a normal distribution. These findings introduced another question: Do the linked inter-landmark distances provide an assessment model for the presence or absence of their associated SNPs? This question was answered through the bootstrap analysis and the predictive profiler statistical assessments associated with the Random Forest Model building. Those tests provide a new approach that can help in the prediction of correlations, the pattern seen in the profile predictor of each ILD's value is distinct where the values have different plateaus according to the relative values of the associated SNPs. This output can be interpreted as an indicator of the categorical nature of the absence and presence of the associated SNPs. This behavior in prediction is notable, especially since some of those variables showed values that can be assessed in future research, such as the prediction profiles of rs9278332, rs80076432, and rs61295642. In other words, the assessment profiles have three distinct patterns, as shown in Figure 9. The first pattern in blue represents a homozygosity at this locus with the minor allele giving a lower value of prosthion- subspinale distance. The second

pattern in purple represents the heterozygosity of this locus (presence of the minor and major alleles). The third allele in green represents the homozygosity at this locus of the major allele, where the value in the assessment profile of the rs8007643 is almost 0; corresponding to a larger distance. Those distinctive patterns are a first statistical representation of a correlation between genetic markers and craniometrics that can be applied in future studies, with the aim that the forensic anthropologist benefit from such model for forensic reconstruction purposes.

The small sample size of this initial project prevented a validation of this analysis by choosing holdout samples for testing and training Bootstrap Forest models. These predictive measurements cannot be directly used when applying this approach on a larger sample to increase accuracy and decrease generalized error (Shao 1996).

After applying correlations on a one-to-one basis, we applied the principal component analysis (PCA) and the pairwise Procrustes test to show potential group correlations. PCA results had a slightly different pattern in sample distribution between ILDs and SNPs, but the overall consistency is present in both groups of variables. This is consistent with the criteria set forth at the beginning of this analysis to evaluate individuals with the same "ancestry", within a defined age range, and absence of facial modifications due to trauma, edentulousness, or congenital condition. The few outliers found in each set of variables is likely a simple representation of human variability within a population (Little et al. 2006) and can be an indication of an individual's unique features that distinguish them from others. But, the correlation on the non-randomness analysis in a symmetric Procrustes test showed no visible correlation on group level because the sum of squares is 0.95 and the correlation is 0.22.

These different tests showed different results that make answering the initial research question about the relationships of SNPs to ILDs a challenge: it cannot be reduced to a simple yes/no answer, in terms of associations between SNPs and ILDs. Yes, there is a correlation

between the SNP markers and craniofacial measurements. However, the associations are not linear correlations as anticipated, but rather hierarchical and multiple. This may be due to the different measurements used on the skull versus those on the living face as reported previously in the literature (Shaffer et al. 2016), but they do correlate to other measurements from other functional groups. There are some SNPs that did not show any type of correlation, but since they showed correlations in previous soft tissue research, this implies that while those SNPs are related to the soft tissue of the face, they are not related to the craniofacial hard tissue (or they can be influenced by environmental factors).

These findings raise an important point, which is the validity of conclusions from previous literature on predictive facial genetics to the application of forensic anthropology work. Since there were similarities and differences between the proposed (expected) correlation and the actual correlation, this suggests that genetic-soft tissues approaches (e.g., Paternoster et al. 2012) can be used to help set a starting point for relationships between genetic markers and craniofacial measurements. However, the soft tissue approaches are not enough to show the different variability and associations each marker expresses on the skull. The fact that the correlated SNPs and ILDs had mostly different functional groups than what was expected shows a hierarchical correlation between several morphologies of the face. This multi-branch correlation affects the morphological structure of the face in more than just a unilateral relationship between two variables. Some of the most recent literature tackled this issue confirming the necessity of observing the association in a multidimensional approach (Claes et al. 2018; White et al. 2019). This difference in morphological groups between SNPs and ILDs raises an obvious concern and future direction: the necessity for more research in forensic anthropology to tackle more validation studies before using any facial models developed by commercial entities, since those predictions do not apply directly to the skull.

Conclusion

This pilot study represents, to our knowledge, the first attempt at integrating the study of genetics and craniometrics for facial approximation purposes. While small in size, analysis of this sample found strong evidence for correlations between individual traits. These results suggest that these findings can be used to reliably support future forensic anthropology research. They also challenge assumptions that genetic associations are sufficiently similar between skull and tissue to warrant the use of the same SNPs in their analysis. We argue, therefore, that more research should access each SNP individually because some of the attributed ones, as seen in this study, failed to be expressed on the hard tissue and may only be related to the soft tissue.

Future research should increase sample sizes, population groups, and additional SNP markers previously claimed to be informative of face shape in the literature, in order to observe these patterns of correlation. The amount of information gathered for the population in this way and the possibility of even linking genetic markers to craniometrics on an individual level can help inform future studies that seek to understand genetic heritability, environmental effects, and plasticity of the skull. Further, the discrepancy observed between the different population markers can be of help in developing new techniques in human identification and forensic facial approximation.

Acknowledgments

We thank the generosity of the donors and their families from the Willed Body Donation Program at the Forensic Anthropology Center at Texas State University. This research was made possible through financial support to the first author from the Fulbright Scholars Program. Genetic sequencing was funded by the Grady E. Early Fellowship and the Kang Laboratory at

Texas State University. We want to acknowledge the help and support of the laboratory's members during the completion of the genetic analysis.

Received 30 March 2021; accepted for publication 3 September 2021.

Literature Cited

Adhikari, K., M. Fuentes-Guajardo, M. Quinto-Sanchez et al. 2016. A genome-wide association scan implicates DCHS2, RUNX2, GLI3, PAX1 and EDAR in human facial variation. *Nat. Commun.* 7:1–11.

Algee-Hewitt, B. F.B. 2016. Population inference from contemporary American craniometrics. *Am. J. Phys. Anthropol.* 160:604–624.

Alvarez-Cubero, M. J., M. Saiz, B. Martínez-García et al. 2017. Next generation sequencing: An application in forensic sciences? *Ann. Hum. Biol.* 44:581–592.

Bajrami, E., and M. Spiroski. 2016. Genomic imprinting. *Open Access Maced. J. Med. Sci.* 4:181–184.

Bonfante, B., P. Faux, N. Navarro et al. 2021. A GWAS in Latin Americans identifies novel face shape loci, implicating VPS13B and a Denisovan introgressed region in facial variation. *Sci. Adv.* 7(6):eabc6160.

Bookstein, F. L. 1997. Landmark methods for forms without landmarks: Morphometrics of group differences in outline shape. *Med. Image Anal.* 1:225–243.

Bryc, K., E. Y. Durand, J. M. Macpherson et al. 2015. The genetic ancestry of African Americans, Latinos, and European Americans across the United States. *Am. J. Hum. Genet.* 96:37–53.

Budowle, B., and A. van Daal. 2008. Forensically relevant SNP classes. *Biotechniques* 44:603–608, 610.

Buschang, P. H., and R. J. Hinton. 2005. A gradient of potential for modifying craniofacial growth. *Semin. Orthod.* 11:219–226.

Cha, S., J. E. Lim, A. Y. Park et al. 2018. Identification of five novel genetic loci related to facial morphology by genome-wide association studies. *BMC Genomics* 19:481.

Chaitanya, L., K. Breslin, S. Zuñiga et al. 2018. The HIrisPlex-S system for eye, hair and skin colour prediction from DNA: Introduction and forensic developmental validation. *Forensic Sci. Int. Genet.* 35:123–135.

Chiego, D. J. 2019. *Essentials of Oral Histology and Embryology: A Clinical Approach*. 5th ed. St. Louis, MO: Elsevier.

Cho, Y. S., M. J. Go, J. Y. Kim et al. 2009. A large-scale genome-wide association study of Asian populations uncovers genetic factors influencing eight quantitative traits. *Nat. Genet.* 41:527–534.

Claes, P., D. K. Liberton, K. Daniels et al. 2014. Modeling 3D facial shape from DNA. *PLoS Genet.* 10:e1004224.

Claes, P., J. Roosenboom, J. D. White et al. 2018. Genome-wide mapping of global-to-local genetic effects on human facial shape. *Nat. Genet.* 50:414–423

Cole, J. B., M. Manyama, J. R. Larson et al. 2017. Human facial shape and size heritability and genetic correlations. *Genetics* 205:967–978.

Deloukas, P., G. D. Schuler, G. Gyapay et al. 1998. A physical map of 30,000 human genes. *Science* 282:744–746.

Desjardins, P., and D. Conklin. 2010. NanoDrop microvolume quantitation of nucleic acids. *J. Vis. Exp.* 45:e2565.

Dougherty, D., and A. Robbins. 1997. *sed & awk: UNIX Power Tools*. 2nd ed. Sebastopol, CA: O'Reilly Media, Inc.

Fortes, G. G., C. F. Speller, M. Hofreiter et al. 2013. Phenotypes from ancient DNA: Approaches, insights, and prospects. *BioEssays* 35:690–695.

GE Healthcare. 2010. *Reliable Extraction of DNA from Whatman™ FTA™ Cards.* Application Note 28-9882-22 AA. Little Chalfont, UK: GE Healthcare.

Gerasimov, M. M. 1971. *The Face Finder*. London: Hutchinson Publishing.

Gupta, S., V. Gupta, H. Vij et al. 2015. Forensic facial reconstruction: The final frontier. *J. Clin. Diagn. Res.* 9:26–28.

Guyomarc'h, P., B. Dutailly, J. Charton et al. 2014. Anthropological facial approximation in three dimensions (AFA3D): Computer-assisted estimation of the facial morphology using geometric morphometrics. *J. Forensic Sci.* 59:1,502–1,516.

Hallgrímsson, B., D. E. Lieberman, W. Liu et al. 2007. Epigenetic interactions and the structure of phenotypic variation in the cranium. *Evol. Dev.* 9:76–91.

Howells, W. 1973. *Cranial Variation in Man: A Study by Multivariate Analysis of Patterns of Difference among Recent Human Populations.* Vol. 67, Papers of the Peabody Museum of Archaeology and Ethnology. Cambridge, MA: Harvard University, Peabody Museum.

Hudson, T. J., L. D. Stein, S. S. Gerety et al. 1995. An STS-based map of the human genome. *Science* 270:1,945–1,954.

Indencleef, K., H. Hoskens, M. K. Lee et al. 2021. The intersection of the genetic architectures of orofacial clefts and normal facial variation. *Front. Genet.* 12:626403.

Kapp-Simon, K. A., D. J. Simon, and S. Kristovich S. 1992. Self-perception, social skills, adjustment, and inhibition in young adolescents with craniofacial anomalies. *Cleft Palate Craniofac. J.* 29:542–356.

Kimmerle, E. H., A. Ross, and D. Slice. 2008. Sexual dimorphism in America: Geometric morphometric analysis of the craniofacial region. *J. Forensic Sci.* 53:54–57.

Klingenberg, C. P. 2011. MorphoJ: An integrated software package for geometric morphometrics. *Mol. Ecol. Resour.* 11:353–357.

Kuhn, R. M., D. Haussler, and W. J. Kent. 2013. The UCSC genome browser and associated tools. *Brief. Bioinform.* 14:144–161.

Langley, N. R., L. M. Jantz, S. D. Ousley et al. 2016. *Data Collection Procedures for Forensic Skeletal Material 2.0*. Knoxville, TN: Forensic Anthropology Center, The University of Tennessee.

Langmead, B., and S. L. Salzberg. 2012. Fast gapped-read alignment with Bowtie 2. *Nat. Methods* 9:357–359.

Lao, O., F. Liu, A. Wollstein et al. 2014. GAGA: A new algorithm for genomic inference of geographic ancestry reveals fine level population substructure in Europeans. *PLoS Comput. Biol.* 10:e1003480.

Lee, W. J., C. M. Wilkinson, H. S. Hwang et al. 2015. Correlation between average tissue depth data and quantitative accuracy of forensic craniofacial reconstructions measured by geometric surface comparison method. *J. Forensic Sci.* 60:572–580.

Li, H. 2011. A statistical framework for SNP calling, mutation discovery, association mapping and population genetical parameter estimation from sequencing data. *Bioinformatics* 27:2,987–2,993.

Lieberman, D. 2011. *The Evolution of the Human Head*. Cambridge, MA: Harvard University Press.

Little, B. B., P. H. Buschang, M. E. P. Reyes et al. 2006. Craniofacial dimensions in children in rural Oaxaca, Southern Mexico: Secular change, 1968–2000. *Am. J. Phys. Anthropol.* 131:127–136.

Liu, F., F. van der Lijn, C. Schurmann et al. 2012. A genome-wide association study identifies five loci influencing facial morphology in Europeans. *PLoS Genet.* 8:e1002932.

Liu, F., K. van Duijn, J. R. Vingerling et al. 2009. Eye color and the prediction of complex phenotypes from genotypes. *Curr. Biol.* 19:192–193.

Liu, X., S. Han, Z. Wang et al. 2013. Variant callers for next-generation sequencing data: A comparison study. *PLoS One* 8:e75619.

Maroñas, O., J. Söchtig, Y. Ruiz et al. 2015. The genetics of skin, hair, and eye color variation and its relevance to forensic pigmentation predictive tests. *Forensic Sci. Rev.* 27:13–40.

Martin, M. 2011. Cutadapt removes adapter sequences from high-throughput sequencing reads. *EMBnet.journal* 17:10–12.

McKinney, W. 2018. *Python for Data Analysis: Data wrangling with Pandas, NumPy, and IPython.* 2nd ed. Sebastopol, CA: O'Reilly Media, Inc.

Mossey, P. A., R. Arngrimsson, J. McColl et al. 1998. Prediction of liability to orofacial clefting using genetic and craniofacial data from parents. *J. Med. Genet.* 5:371.

Ousley, S. 2004. *3Skull Computer Program.* Version 2:111.

Parabon NanoLabs. 2016. *Workflow of a Parabon® Snapshot™ Investigation.* Reston, VA: Parabon NanoLabs, Inc.

Paternoster, L., A. I. Zhurov, A. M. Toma et al. 2012. Genome-wide association study of three-dimensional facial morphology identifies a variant in PAX3 associated with nasion position. *Am. J. Hum. Genet.* 90:478–485.

Peng, S., J. Tan, S. Hu et al. 2013. Detecting genetic association of common human facial morphological variation using high density 3D image registration. *PLoS Comput. Biol.* 9:e1003375.

Phipps, A., and H. Larry, eds. 1996. *Clustering and Classification*. River Edge, NJ: World Scientific Publishing Co.

R Core Team. 2016. *R: A Language and Environment for Statistical Computing.* Vienna: R Foundation for Statistical Computing. https://www.R-project.org.

Reijnders, M. R. F., K. A. Miller, M. Alvi et al. 2018. De novo and inherited loss-of-function variants in TLK2: Clinical and genotype-phenotype evaluation of a distinct neurodevelopmental disorder. *Am. J. Hum. Genet.* 102:1,195–1,203.

Relethford, J. H. 2016. Biological distances and population genetics in bioarchaeology. In *Biological Distance Analysis*, M. A. Pilloud and J. T. Hefner, eds. San Diego, CA: Academic Press, 23–33.

Retzlaff, E. W. 1987. Embryological development of the cranium. In *The Cranium and Its Sutures: Anatomy, Physiology, Clinical Applications and Annotated Bibliography of Research in the Cranial Field*, E. W. Retzlaff and F. L. Mitchell, eds. Berlin, DE: Springer-Verlag, 1–4.

Sakuma, A., M. Ishii, S. Yamamoto et al. 2010. Application of postmortem 3D-CT facial reconstruction for personal identification. *J. Forensic Sci.* 55:1,624–1,629.

Sall, J., A. Lehman, M. L. Stephens et al. 2012. *JMP Start Statistics: A Guide to Statistics and Data Analysis using JMP*. 5th ed. Cary, NC: SAS Institute.

Schoenwolf, G. C., S. B. Bleyl, P. R. Brauer et al. 2015. *Larsen's Human Embryology*. 5th ed. New York: Elsevier.

Shaffer, J. R., E. Orlova, M. K. Lee et al. 2016. Genome-wide association study reveals multiple loci influencing normal human facial morphology. *PLoS Genet.* 12:e1006149.

Shao, J. 1996. Bootstrap model selection. *J. Am. Stat. Assoc.* 91:655–665.

Sholts, S. B., S. K. Warmlander, L. M. Flores et al. 2010. Variation in the measurement of cranial volume and surface area using 3D laser scanning technology. *J. Forensic Sci.* 55:871–876.

Stewart, E. A., K. B. McKusick, A. Aggarwal et al. 1997. An STS-based radiation hybrid map of the human genome. *Genome Res.* 7:422–433.

Taylor, K. T. 2001. *Forensic Art and Illustration*: Boca Raton, FL: CRC Press.

Toomey, D. 2016. *Learning Jupyter*. Birmingham, UK: Packt Publishing Ltd.

Untergasser, A., I. Cutcutache, T. Koressaar et al. 2012. Primer3—new capabilities and interfaces. *Nucleic Acids Res.* 40:e115.

Walker, P. L. 2008. Sexing skulls using discriminant function analysis of visually assessed traits. *Am. J. Phys. Anthropol.* 136:39–50.

Walsh, S., L. Chaitanya, L. Clarisse et al. 2014. Developmental validation of the HIrisPlex system: DNA-based eye and hair colour prediction for forensic and anthropological usage. *Forensic Sci. Int. Genet.* 9:150–161.

Walsh, S., F. Liu, A. Wollstein et al. 2012. The HIrisPlex system for simultaneous prediction of hair and eye colour from DNA. *Forensic Sci. Int. Genet.* 7:98–115.

White, J. D., J. Roosenboom, K. Indencleef et al. 2019. Meta-analysis identifies 48 SNPs with multiple independent effects on human facial features. *Am. J. Phys. Anthropol.* 168:267.

White, T. D., M. T. Black, and P. A. Folkens. 2012. *Human Osteology*. 3rd ed. Boston, MA: Academic Press.

Wilkinson, C. 2004. *Forensic Facial Reconstruction*. Cambridge, MA: Cambridge University Press.

Young, N. M., D. Hu, A. J. Lainoff et al. 2014. Embryonic bauplans and the developmental origins of facial diversity and constraint. *Development* 141:1,059–1,063.

Table 1. The 99 Skull Landmarks and Their Respective Numbering Shown in Figure 1

#	Abrv	LANDMARK	#	Abrv	LANDMARK
1	prosH	Prosthion-Howells	50	mplr	Marginal Process Lateral R
2	prosM	Prosthion-Martin	51	jugr	Jugale R
3	ssp	Subspinale	52	nas	Nasion
4	alarl	Alare L	53	glb	Glabella
5	nlhil	Most Inferior Nasal Border L	54	spglb	Supraglabellare
6	nlhir	Most Inferior Nasal Border R	55	brg	Bregma
7	alarr	Alare R	56	mastl	Mastoideale L
8	wmhil	Cheek Height Inf Point L	57	aubl	Radiculare L (Zyg Root)
9	wmhsl	Cheek Height Sup Point R	58	aubr	Radiculare R (Zyg Root)
10	obhsl	Upper Orbital Border L	59	radptl	Radiometer Point L
11	obhil	Lower Orbital Border L	60	porr	Porion R
12	zygool	Zygoorbitale L	61	mastr	Mastoideale R
13	nasil	Nasale Inferius L	62	hor	Hormion
14	nasir	Nasale Inferius R	63	alv	Alveolon (Rubber Band)
15	zygoor	Zygoorbitale R	64	staur	Staurion
16	obhir	Lower Orbital Border R	65	ecml	Ectomolare L
17	obhsr	Upper Orbital Border R	66	avrptl	M1 Anterior Point L
18	wmhsr	Cheek Height Sup Point L	67	ecmr	Ectomolare R
19	wmhir	Cheek Height Inf Point R	68	malapt	Pogonion (Mand Length)
20	ectl	Ectoconchion L	69	gniipt	Gnathion
21	dacl	Dacryon L	70	gnispt	Infradentale
22	nassl	Nasale Superius L	71	hmfiptl	HMF Inf Pt L
23	wnbl	Nasomaxillary Suture Pinch L	72	hmfsptl	HMF Sup Pt L
24	wnbr	Nasomaxillary Suture Pinch R	73	tmfbptl	TMF Buccal Pt L
25	nassr	Nasale Superius R	74	tmflptl	TMF Lingual Pt L
26	dacr	Dacryon R	75	gonl	Gonion L
27	ectr	Ectoconchion R	76	hmfiptr	HMF Inf Pt R
28	zygr	Zygion R	77	imnptl	Inferior Mandibular Notch L
29	zytil	Zygotemporale Inferior R	78	coronl	Coronion L
30	zytsl	Zygotemporale Superior R	79	latcndl	Condylion Laterale L
31	zygomr	Zygomaxilare R	80	supcndlP	L Sup Condyle Post
32	zygoml	Zygomaxilare L	81	medcndl	Condylion Mediale L
33	zytsr	Zygotemporale Superior L	82	medcndr	Condylion Mediale R
34	zytir	Zygotemporale Inferior L	83	supcndrP	R Sup Condyle Post
35	zygl	Zygion L	84	imnptr	Inferior Mandibular Notch R
36	jugl	Jugale L	85	latcndr	Condylion Laterale R

37	mpll	Marginal Process Lateral L	86	coronr	Coronion R
38	fmtl	Frontomalare Temporale L	87	ans	Anterior Nasal Spine
39	fmal	Frontomalare Anterior L	88	gonr	Gonion R
40	wfbl	Frontotemporale L	89	wrbapt	WRB Posterior Pt
41	krol	Krotaphion L	90	wrbppt	WRB Anterior Pt
42	xfbl	Maximum Frontal Point L	91	sispt	Nasal Bone Elevation
43	stpl	Stephanion L	92	ndspt	Deepest Point On Nasal
44	stpr	Stephanion R	93	radptr	Radiometer Point R
45	xfbr	Maximum Frontal Point R	94	porl	Porion L
46	kror	Krotaphion R	95	avrptr	M1 Anterior Point R
47	wfbr	Frontotemporale R	96	hmfsptr	HMF Sup Pt R
48	fmar	Frontomalare Anterior R	97	tmfbptr	TMF Buccal Pt R
49	fmtr	Frontomalare Temporale R	98	tmflptr	TMF Lingual Pt R
			99	chpp	Chin Protrusion Point

Table 2. Presence/Absence of SNPs in Each Sample, according to the Bioinformatic Analysis (1=present, 0=absent)

Willed body donor numbers.

	D36-2012	D17-2013	D60-2015	D24-2013	D31-2015	D41-2015	D27-2012	D20-2012	D38-2012	D15-2014	D22-2013	D49-2014	D39-2012	D55-2013	D14-2013	D57-2014	D60-2014	**Total**
rs72691108	1	1	1	1	1	1	0	1	0	0	0	0	1	0	0	1	0	**9**
rs4648379	0	0	0	0	0	0	1	0	1	0	0	1	1	0	0	0	0	**4**
rs12786942	0	0	1	0	0	0	0	0	0	0	1	0	0	0	1	0	0	**3**
rs10862567	0	0	0	0	0	0	0	0	0	0	0	0	0	0	0	0	0	**0**
rs8007643	0	0	0	0	0	0	0	0	0	0	0	1	0	1	0	0	0	**2**
rs17106852	0	0	0	0	1	0	1	1	0	0	0	0	0	1	0	0	0	**4**
rs7559271	0	0	0	0	0	0	0	0	0	0	0	0	0	0	0	0	0	**0**
rs3827760	0	0	0	0	0	0	0	0	0	0	0	0	0	0	0	0	0	**0**
rs6740960	0	0	0	0	0	0	0	0	0	0	0	0	0	0	0	0	0	**0**
rs6129564	0	0	1	0	0	0	0	0	0	1	0	0	0	0	0	0	0	**2**
rs927833	0	0	0	0	1	0	0	0	0	0	0	0	0	1	0	0	0	**2**
rs17447439	0	0	0	0	0	0	0	0	0	0	0	0	0	0	0	0	0	**0**
rs1982862	0	0	0	0	0	0	0	0	0	0	0	0	0	0	1	1	0	**2**
rs2977562	1	0	0	0	1	1	0	1	0	1	1	1	1	1	0	1	0	**10**
rs9995821	1	0	1	0	0	0	0	0	0	1	1	1	0	1	0	1	1	**8**
rs11738462	1	0	0	1	0	1	0	0	0	0	0	0	1	0	1	0	1	**6**
rs6555969	0	0	0	0	0	0	0	0	0	0	0	0	0	0	0	0	0	**0**
rs5880172	0	0	0	0	0	0	0	0	0	0	0	0	0	0	0	0	0	**0**
rs17640804	0	0	0	0	0	0	0	0	0	0	0	0	0	0	0	0	0	**0**
rs10238953	0	0	0	0	0	0	0	0	0	0	0	0	0	0	0	0	0	**0**

Table 3. Spearman's Correlation between the SNPs and ILDs, with a p-value < 0.05

Blue grade colors represent the values of rho, the light blue represents a negative correlation, the dark blue represents a positive correlation. Pink grade colors represent the p-values. The lighter the pink coloration represents a lower p-value.

		Nasal Ala length (L &R)		Cranial width		Nasal Ala length (L &R)		Nasal Ala length (L &R)		Cranial width		Eye-Nasion-Eye		Nasal Ala length (L &R)		Nose wing breadth		Nose tip	
	SNP / ILD	rs11738462		rs171 68522		rs19828623		rs46483792		rs61295642		rs72691108		rs80076432		rs9278332		rs9995829	
philtrum width	alarl-ans															-0.5217	0.0317		
philtrum width,Nasal Ala length (L &R)	alarr-ans																	0.5052	0.0386
Nasal Ala length (L &R)	ans-alarl															-0.5217	0.0317		
philtrum width	ans-prosH							0.6228	0.0076										
philtrum width	ans-prosM							0.6228	0.0076										
philtrum width	ans-ssp							0.5944	0.0118	-0.4845	0.0487								
Eye-Nasion-Eye	dacl-dacr	-0.5528	0.0214																
Eye-Nasion-Eye	dacr-dacl	-0.5528	0.0214																
Eye-Nasion-Eye	fmal-fmar	-0.5276	0.0295																
Chin protrusion	gniipt-chpp									0.559	0.0197								
Chin protrusion	gnispt-gniipt											-0.6014	0.0107						
Chin protrusion	gnispt-malapt											-0.5533	0.0212						

Chin protrusion	**hmfsptr-malapt**							**0.5095**	**0.0367**										
Nasal Ala length (L &R)	**nasil-alarl**	**0.5025**	**0.0398**																
Nasal Ala length (L &R)	**nasir-alarr**			**-0.5944**	**0.012**														
Zygion-Nasion-Zygion	**nas-zygl**																	**0.5052**	**0.0386**
Nose tip,philtrum width,Nasal Ala length (L &R)	**nlhil-ans**			**-0.5378**	**0.026**											**-0.4845**	**0.0487**		
Nose tip	**nlhil-ssp**			**-0.5944**	**0.012**													**0.5774**	**0.0152**
Nose tip,philtrum width,Nasal Ala length (L &R)	**nlhir-ans**																	**0.5292**	**0.0289**
Nose tip	**nlhir-ssp**					**0.5217**	**0.0317**			**-0.4845**	**0.0487**								
Eye-Nasion-Eye	**obhil-obhir**	**-0.5025**	**0.0398**																
philtrum width	**prosH-ssp**											**-0.4845**	**0.0487**						
philtrum width	**prosM-ssp**					**-0.4845**	**0.0487**												
Cranial width	**rs1716852**															**0.6583**	**0.0041**		
Nasal Ala length (L &R)	**sispt-alarl**																	**0.5052**	**0.0386**

Nasal Ala length (L &R)	**sispt-alarr**													**0.5052**	**0.0386**
Nose tip	**ssp-ans**					**0.5944**	**0.0118**	**-0.4845**	**0.0487**						
Cranial width	**stpl-stpr**									**-0.6014**	**0.0107**				
Chin protrusion	**tmflptr-malapt**							**-0.4845**	**0.0487**						
Chin protrusion	**tmflptr-tmflptl**												**0.559**	**0.0197**	
Cranial width	**xfbl-xfbr**									**-0.5052**	**0.0386**			**0.6014**	**0.0107**
Eye-Nasion-Eye	**zygoor-nas**													**0.5052**	**0.0386**
Zygion-Nasion-Zygion	**zygr-nas**									**-0.6495**	**0.0048**				
Zygion-Nasion-Zygion	**zygr-zygl**			**0.4845**	**0.0487**										

Table 4. Bootstrap Analysis Results according to Individually Correlated Variables

Single nucleotide polymorphism (SNP)	Inter-Landmark distances (ILD) used	RSquare	Root mean square error (RMSE)
rs11738462	dacl-dacr dacr-dacl fmal-fmar nasil-alarl obhil-obhir	0.49	0.34
rs17106852	nasir-alarr nlhil-ans nlhil-ssp	0.43	0.32
rs1982862	nlhir-ssp prosM-ssp zygr-zygl	0.45	0.24
rs4648379	ans-prosH ans-prosM ans-ssp hmfsptr-malapt ssp-ans	0.57	0.28
rs6129564	ans-ssp gniipt-chpp nlhir-ssp ssp-ans tmflptr-malapt	0.41	0.25

rs72691108	gnispt-gniipt gnispt-malapt stpl-stpr xfbl-xfbr zygr-nas	0.59	0.32
rs8007643	prosH-ssp	0.35	0.26
rs927833	alarl-ans ans-alarl nlhil-ans tmflptr-tmflptl	0.47	0.23
rs9995821	alarr-ans nas-zygl nlhil-ssp nlhir-ans sispt-alarl sispt-alarr xfbl-xfbr zygoor-nas	0.63	0.3

Table 5. Prediction Profiles of the Different Significant Single Nucleotide Polymorphisms and Their Associated Inter-Landmark Distances

1)

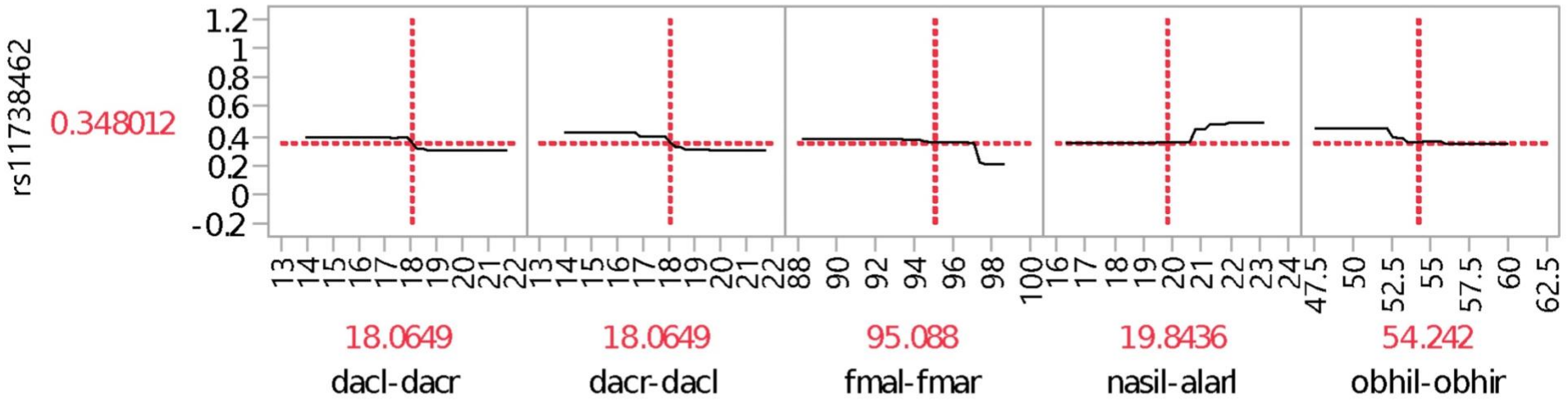

2)

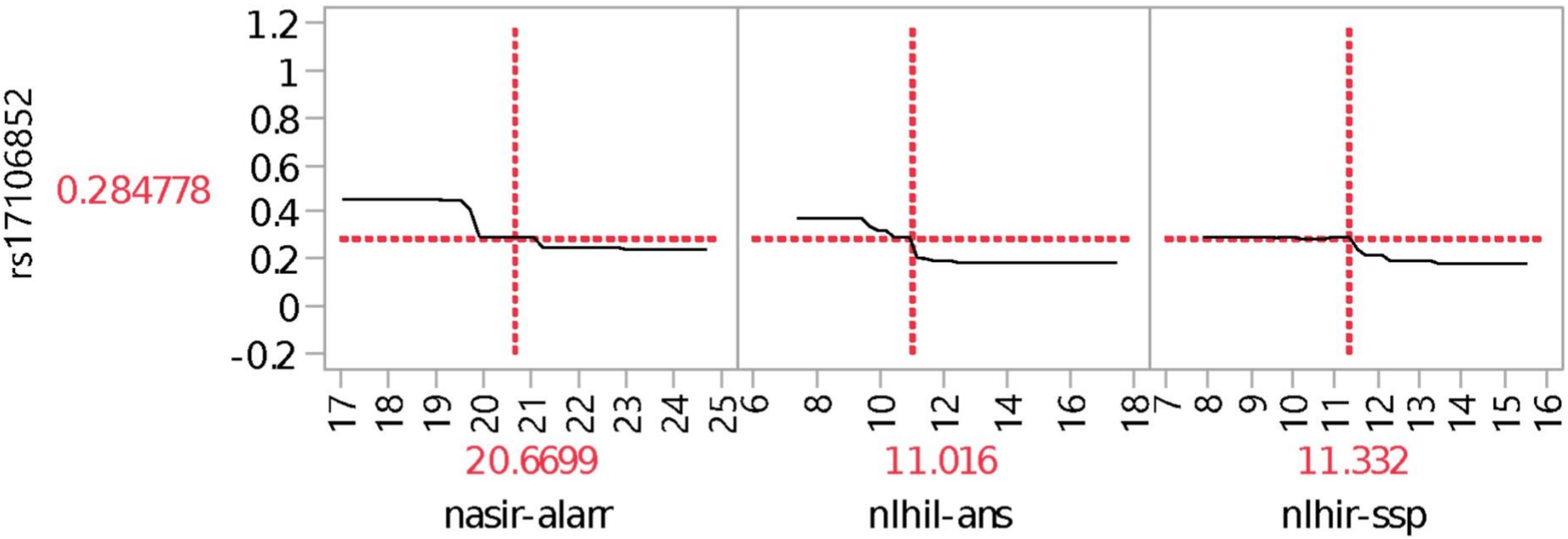

3)

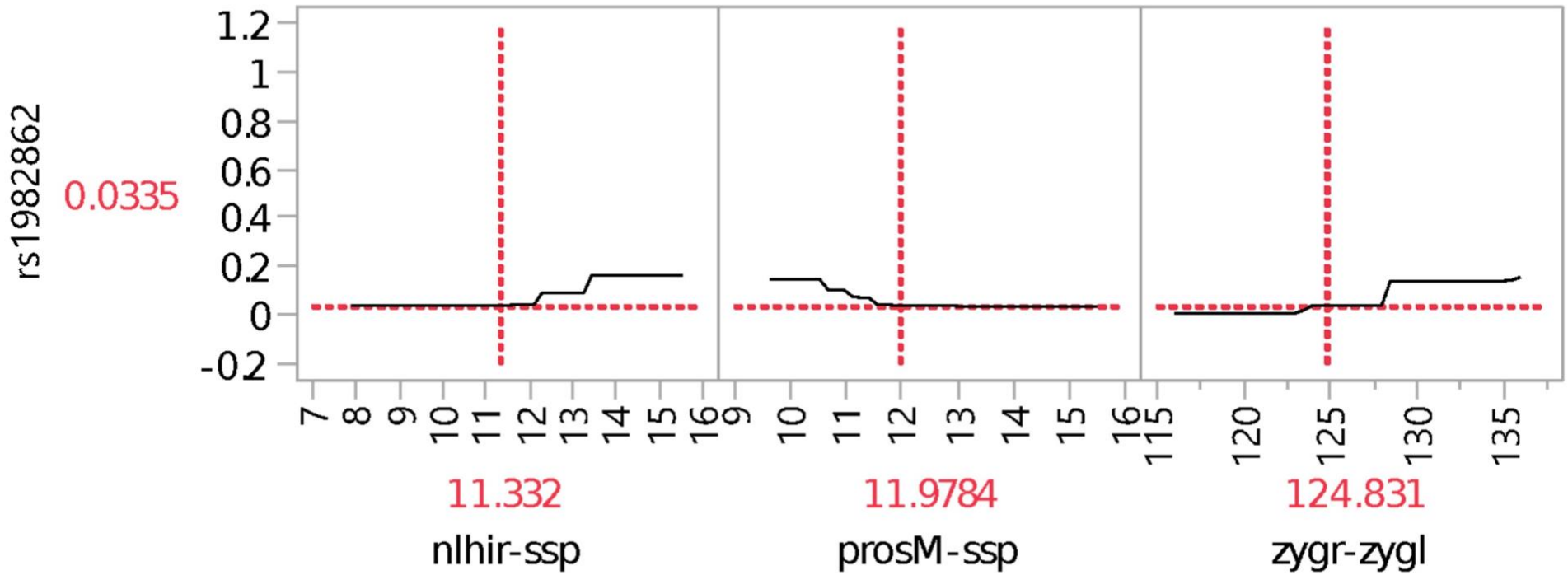

4)

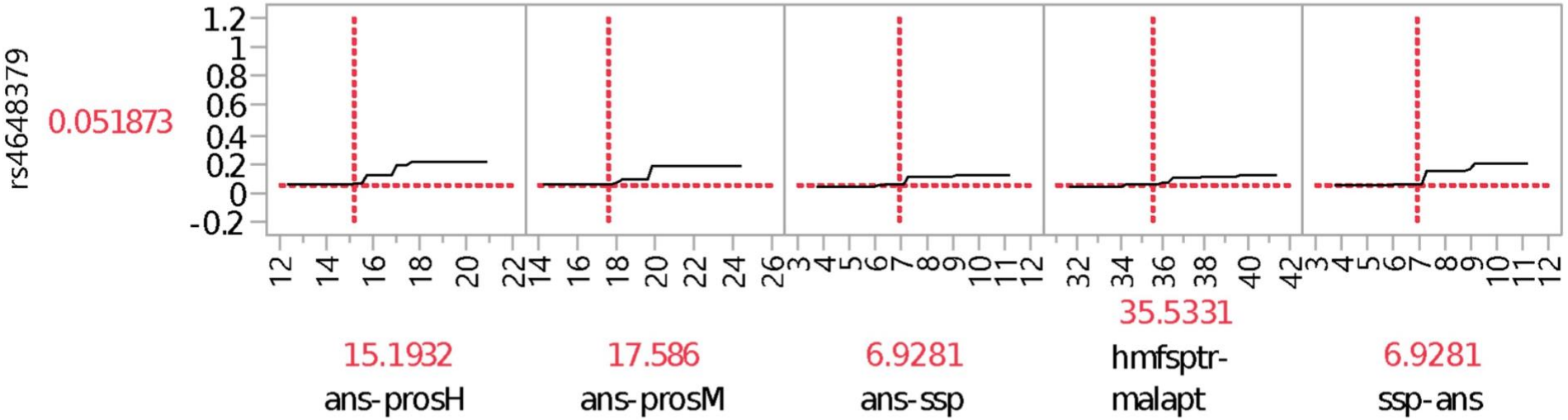
rs4648379
0.051873
1.2
1
0.8
0.6
0.4
0.2
0
-0.2
12 14 16 18 20 22
14 16 18 20 22 24 26
3 4 5 6 7 8 9 10 11 12
32 34 35.5331 38 40 42
3 4 5 6 7 8 9 10 11 12
15.1932
ans-prosH
17.586
ans-prosM
6.9281
ans-ssp
hmfsptr-
malapt
6.9281
ssp-ans

5)

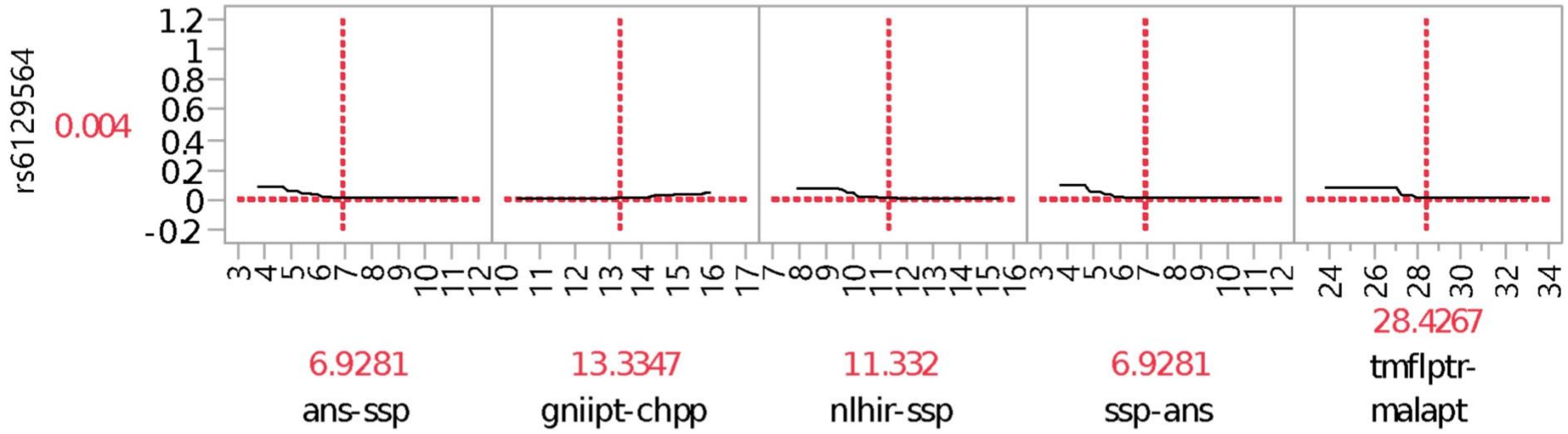
rs6129564
0.004
1.2
1
0.8
0.6
0.4
0.2
0
-0.2
3 4 5 6 7 8 9 10 11 12
10 11 12 13 14 15 16 17
7 8 9 10 11 12 13 14 15 16
3 4 5 6 7 8 9 10 11 12
24 26 28 30 32 34
28.4267
6.9281
ans-ssp
13.3347
gniipt-chpp
11.332
nlhir-ssp
6.9281
ssp-ans
tmflptr-
malapt

6)

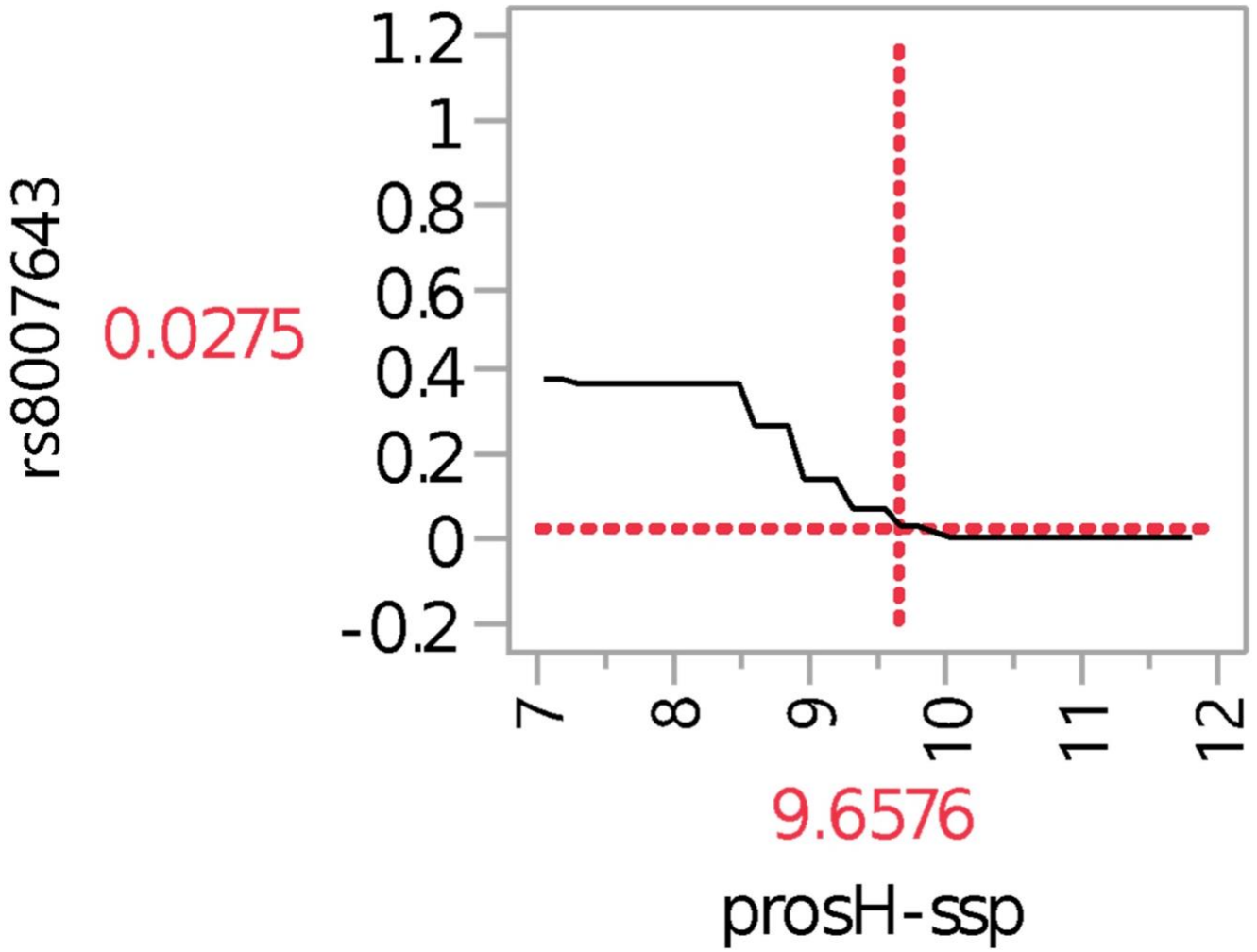

7)

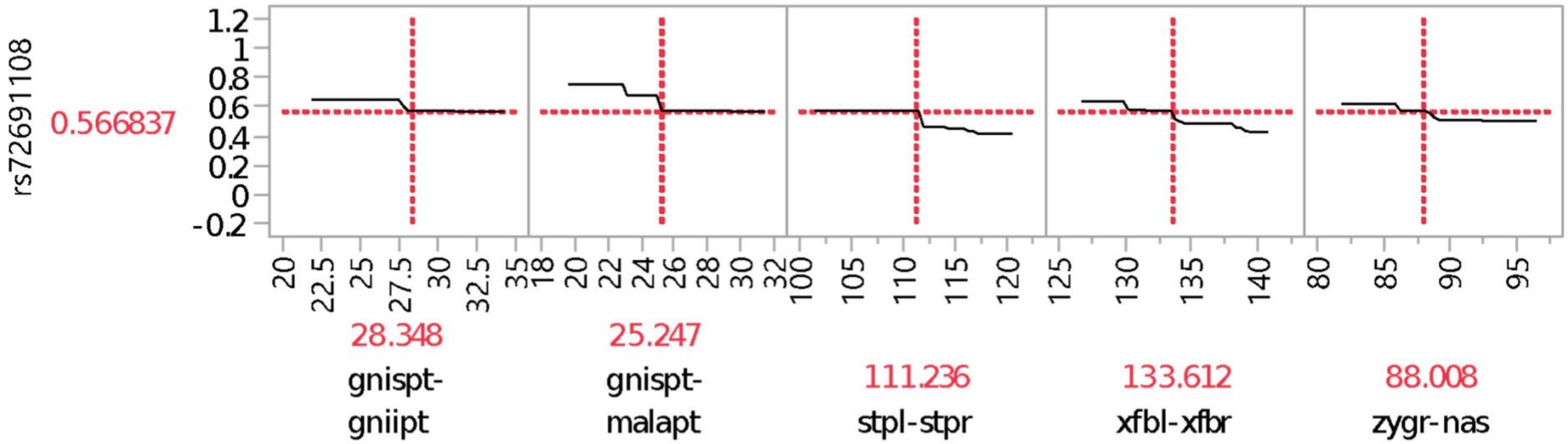

8)

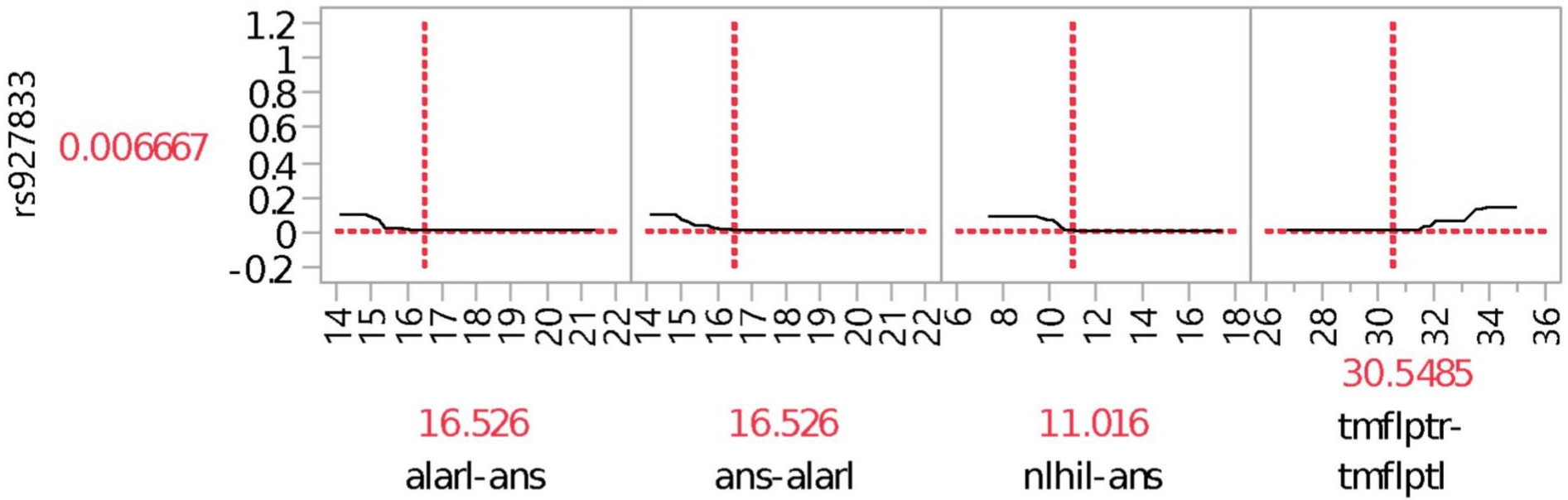

9)

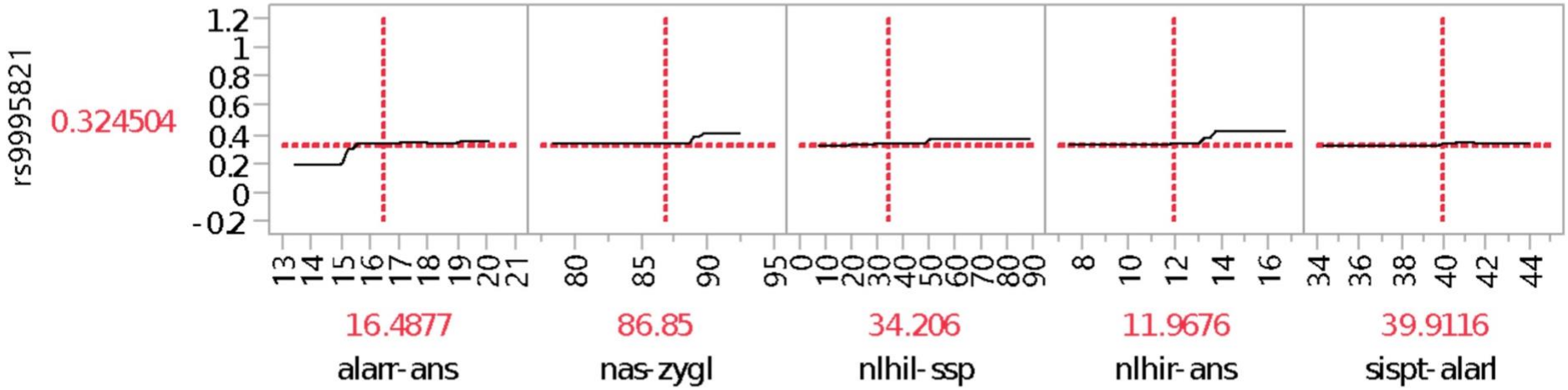
rs9995821
0.324504
1.2
1
0.8
0.6
0.4
0.2
0
-0.2
16.4877
alarr-ans
86.85
nas-zygl
34.206
nlhil-ssp
11.9676
nlhir-ans
39.9116
sispt-alarl

10)

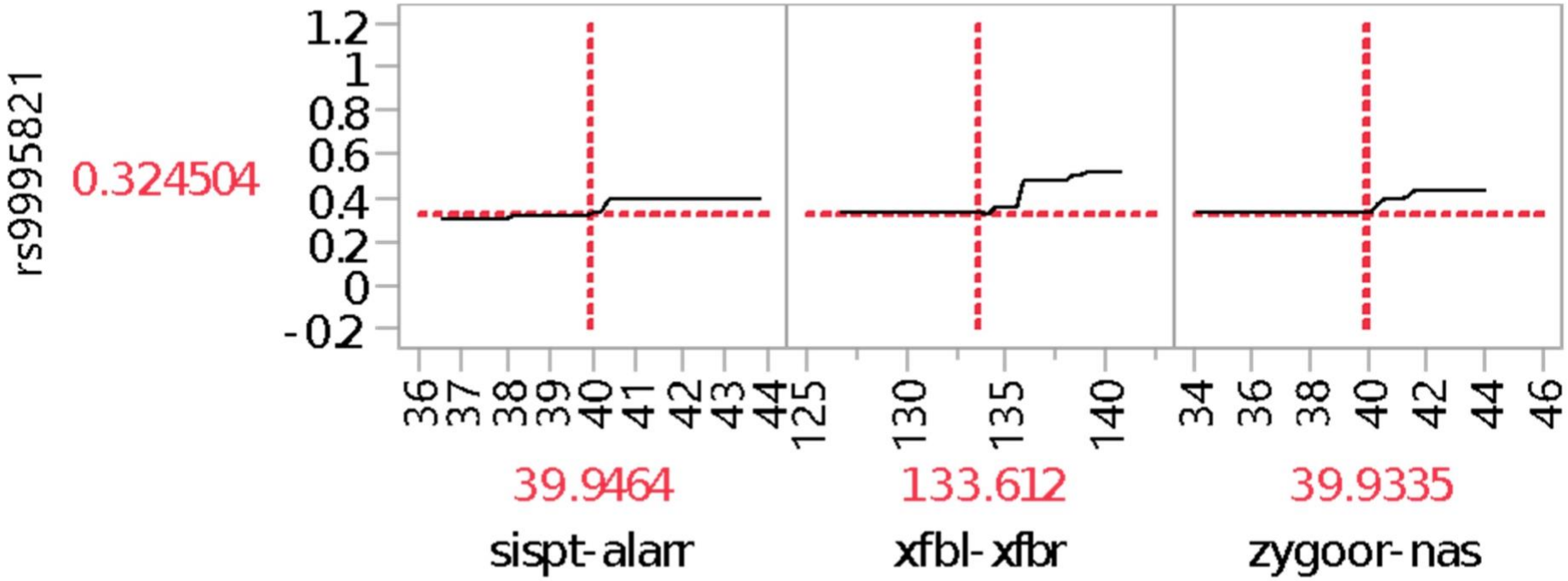

Table 6. The Results of Pair-Wise Procrustes Analysis between ILDs and SNPs

	ILDs to SNPs Sum of squares	ILDs to SNPs Correlation in a symmetric Procrustes rotation	ILDs to SNPs Significance	ILDs to SNPs Permutations
All Individuals	0.952910462	0.217001241	0.759	999

Supplementary Table S1. Selected SNPs Used for This Pilot Study with Their Chromosome Location and Their Associated Trait as Found in Previous Literature

SNP: Single nucleotide polymorphism; Chr: Chromosome.

SNP	Chr	Associated Trait	Reference Article
rs17447439	chr3	Left Eye To Right Eye	(Liu et al. 2012) (Shaffer et al. 2016) (Claes et al. 2018)
rs72691108	chr1	Right /Left Eye To Nasion-Upper facial quadrant	(Claes et al. 2018)
rs7559271	chr2	Nasion To Mid-Endocanthion Point/Nasion Position	(Shaffer et al. 2016) (Paternoster et al. 2012) (Claes et al. 2018) (Adhikari et al)
rs11738462	chr5	Pronasale To Left Alare	(Shaffer et al. 2016) (Paternoster et al. 2012) (Claes et al. 2018)
rs8007643	chr14	Nasal Ala Length	(Claes et al. 2018) (Shaffer et al. 2016)
rs1982862	chr3	Pronasale To Left Alare	(Shaffer et al. 2016) (Paternoster et al. 2012) (Claes et al. 2018)
rs4648379	chr1	Pronasale To Left/Right Alare// Nasal Ala Length	(Liu et al. 2012) (Shaffer et al. 2016) (Claes et al. 2018)
rs6555969	chr5	Left/Right Zygion To Nasion// Right /Left Eye To Nasion	(Liu et al. 2012) (Shaffer et al. 2016) (Claes et al. 2018)
rs12786942	chr11	Upper facial depth	(Shaffer et al. 2016)
rs10862567	chr12	Right Endocanthion In Yz Direction	(Shaffer et al. 2016) (Paternoster et al. 2012) (Claes et al. 2018)
rs17106852	chr14	Cranial base width	(Claes et al. 2018) (Shaffer et al. 2016)
rs6129564	chr20	Cranial Base Width	(Claes et al. 2018) (Shaffer et al. 2016)
rs3827760	chr2	Chin Protrusion	(Adhikari et al. 2016; Claes et al. 2018)
rs6740960	chr2	mandible/chin	(Claes et al. 2018)
rs927833	chr20	Nose Wing Breadth	(Adhikari et al. 2016; Claes et al. 2018)
rs17640804	chr7	Nose Wing Breadth	(Adhikari et al. 2016; Claes et al. 2018)
rs2977562	chr3	Nose Wing Breadth/ philtrum	(Claes et al. 2018)
rs5880172	chr6	Forehead	(Claes et al. 2018)
rs9995821	chr4	Columella/Nose Tip--columella inclination	(Claes et al. 2018)

rs10238953	chr7	mandible and chin	(Claes et al. 2018)

Supplementary Table S2. Table of Eigenvalues of the Frontal Arc (Principal Component Analysis: PCA: CovMatrix, frontal arc, Procrustes coordinates)

	Eigenvalues	% Variance	Cumulative %
1.	0.00101790	54.175	54.175
2.	0.00024092	12.822	66.997
3.	0.00016505	8.784	75.781
4.	0.00009765	5.197	80.978
5.	0.00008897	4.735	85.713
6.	0.00006532	3.476	89.190
7.	0.00004959	2.639	91.829
8.	0.00004145	2.206	94.035
9.	0.00002778	1.478	95.513
10.	0.00002200	1.171	96.685
11.	0.00001526	0.812	97.497
12.	0.00001369	0.729	98.225
13.	0.00001152	0.613	98.838
14.	0.00000992	0.528	99.366
15.	0.00000631	0.336	99.702
16.	0.00000560	0.298	100.000
Total variance: 0.00187893			

Figure Captions

Figure 1. Frontal (on upper left), lateral (on lower the right) view, Inferior view respectively of the skull (on lower left), and anterior view of the mandible (on lower right) with the corresponding landmarks (courtesy of Artist Grace Anderson).

Figure 2. Functional groups with associated SNPs. On the left, the different morphological functional groups are colored on the cranium according to their section number. The table summarizes the different sections with their associated function group and SNP. The figure on the right represents the 99 landmarks and all the inter-landmark distances used.

Figure 3. The distribution of variation among the samples in a 2D representation, using the first two principal components of the cranial landmarks data.

Figure 4. Heat map with the correlation between all the inter-landmark distances and the targeted SNPs. Three distinct correlation patterns are visible. The first one is the absence of correlation, which is represented by 0 (in white). The second pattern is positive correlation ($0<x<1$); and the third pattern is the negative correlation ($-1<x<0$).

Figure 5. The distribution of rho values is shown with the corresponding ILDs.

Figure 6. Principal component analysis providing a distribution of the significant ILDs.

Figure 7. Two-way hierarchical clustering of the significant SNPs and ILDs against the clustering among the donated individuals used in this study.

Figure 8. An example of the Procrustes coordinates with the sum of squares and its tangent from all the coordinates of the frontal arc divided according to the sex of the individuals. The grey represents the numbers of landmarks forming the frontal arc (100), and the black represents the landmark points and the direction of deviation from the total mean.

Figure 9. The prediction profile of rs8007643 where the different stages are highlighted. The circle on the left corresponds to the presence of the SNP, the circle on the right corresponds to the absence of the SNP, and the rectangle in the middle corresponds to the heterozygosity at the alleles at this position.

Figure 1.

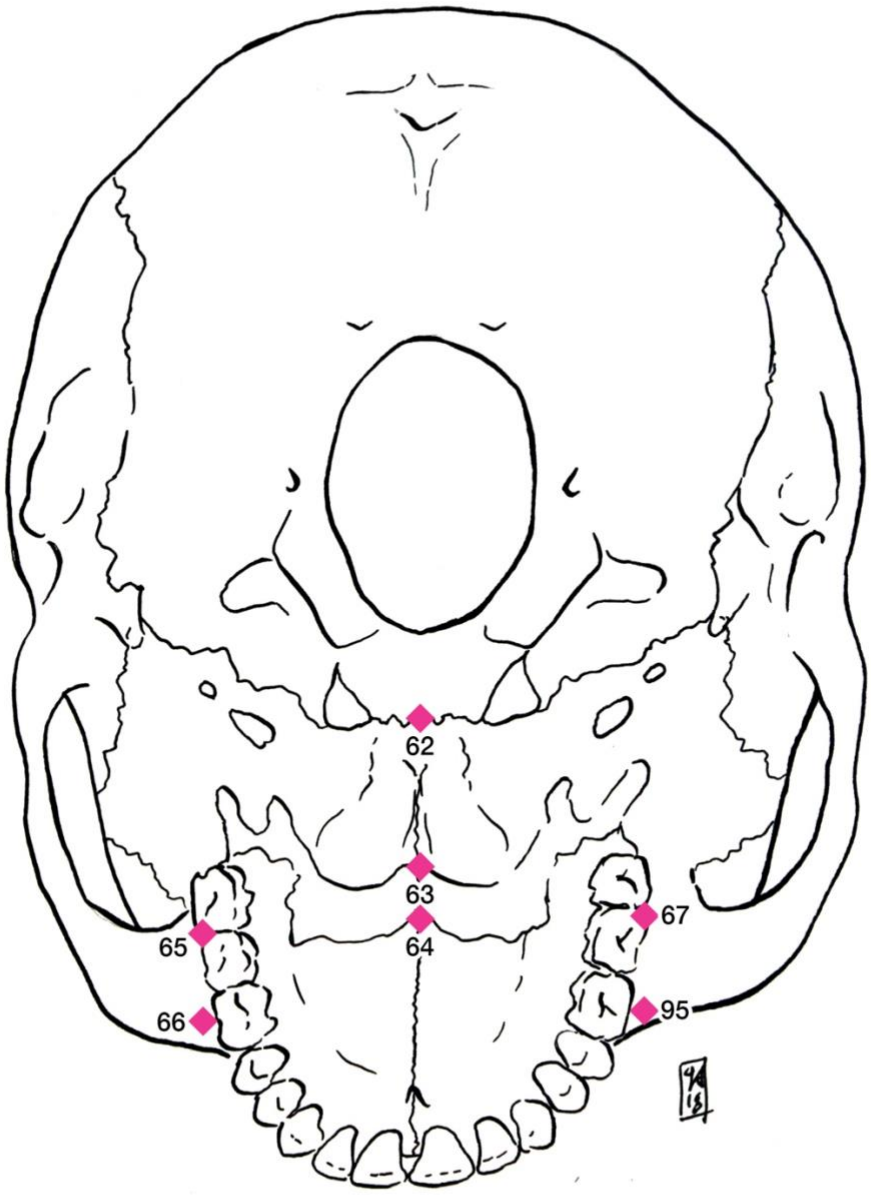

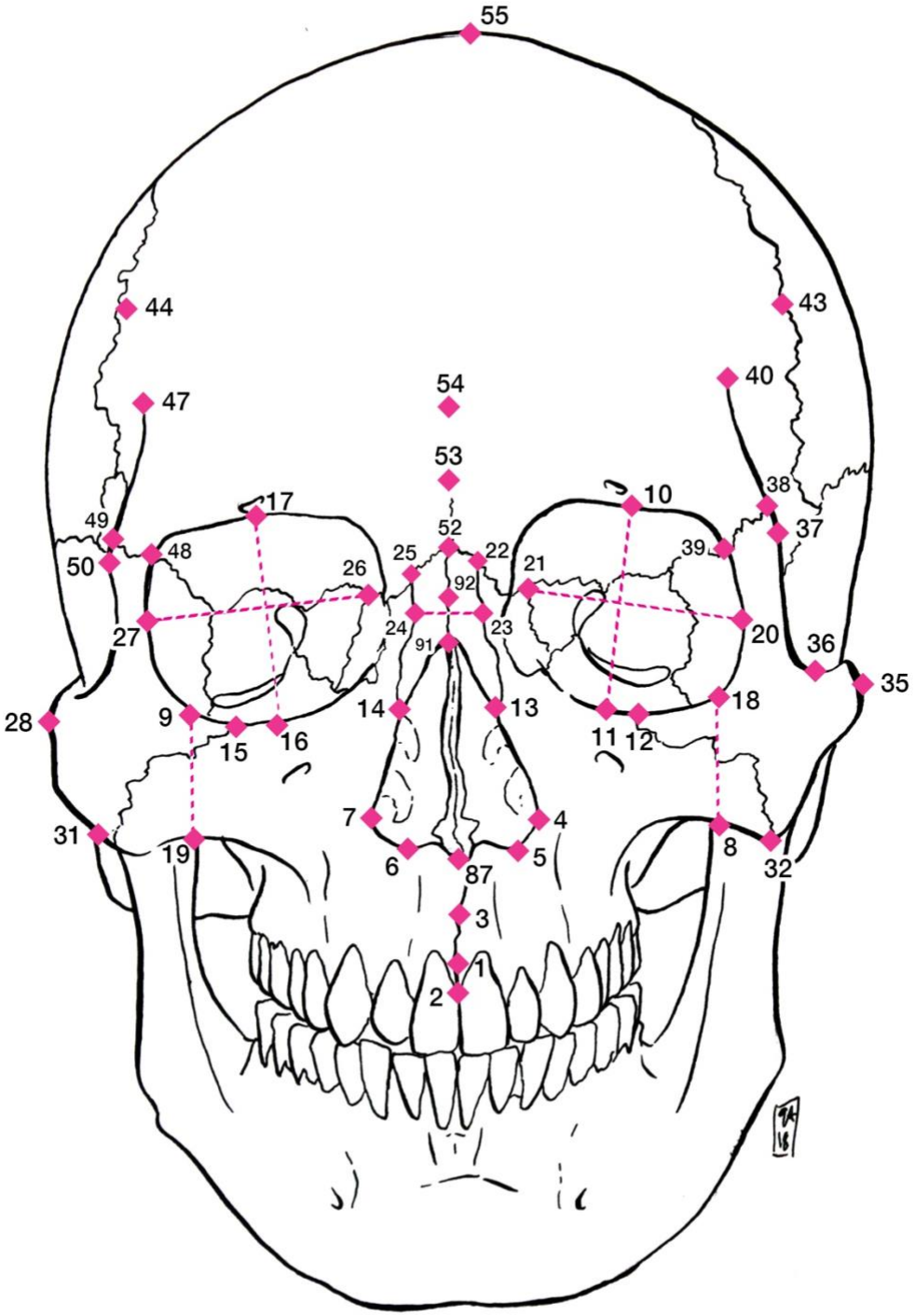

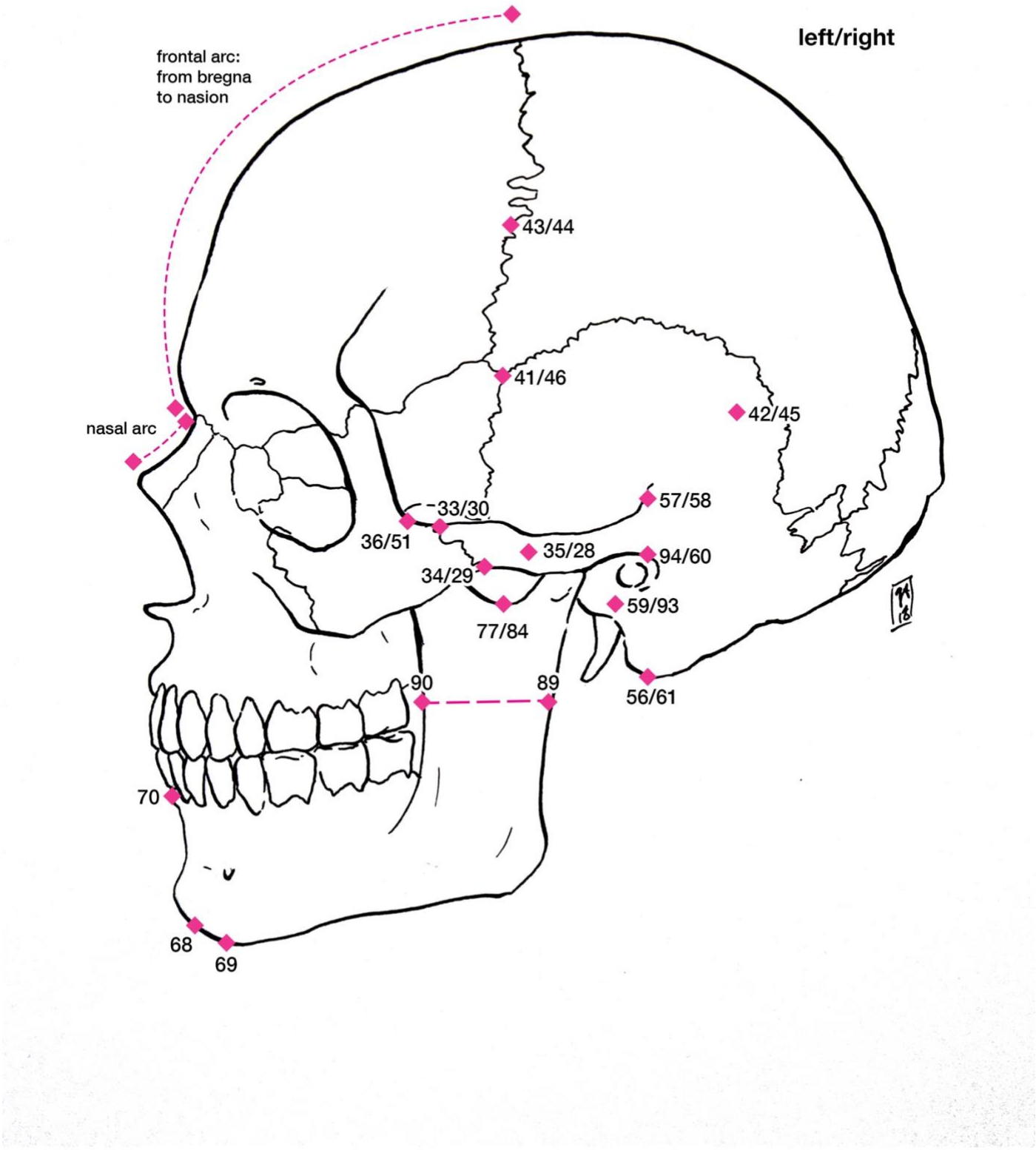

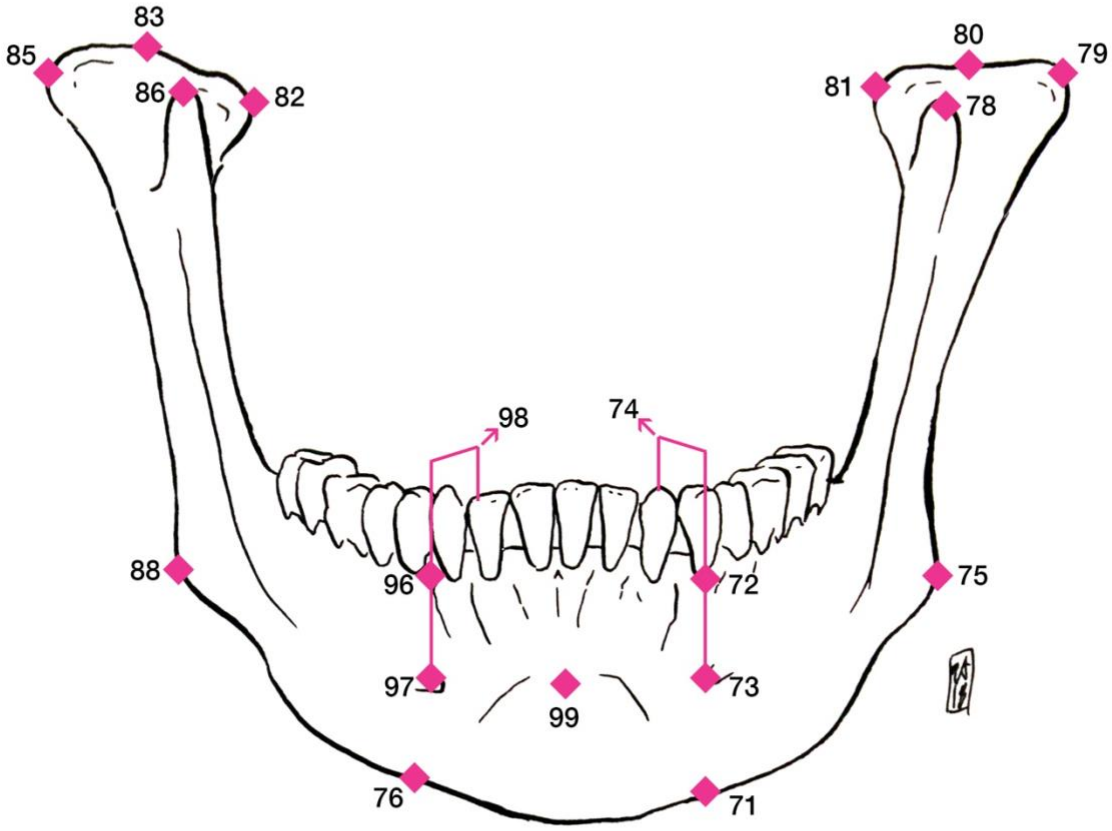

Figure 2.

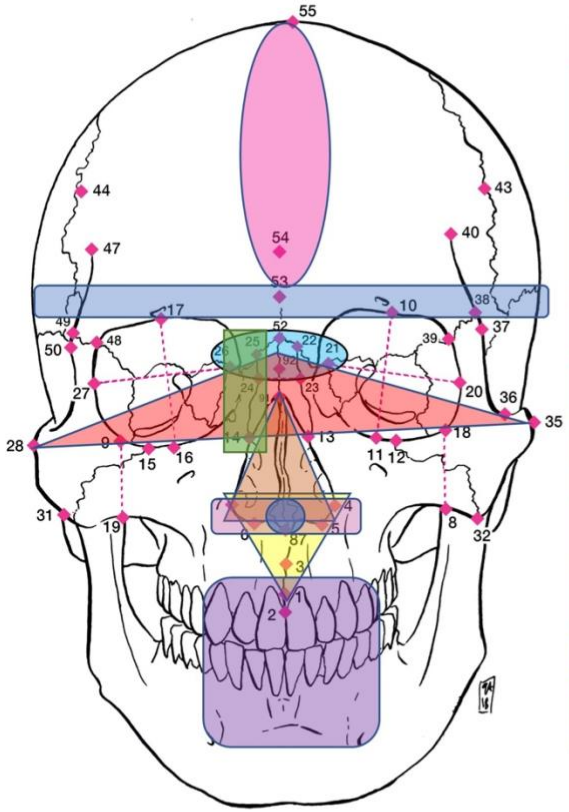

Section	Function group	SNP
Section 1	Eye-Nasion- Eye	rs72691108 rs6555969 rs7559271 rs17447439
Section 2	Nasal Ala length (L &R)	rs4648379 rs8007643 rs1982862 rs11738462
Section 3	Zygion-Nasion-Zygion	rs12786942 rs6555969
Section 4	R endocation in space	rs10862567
Section 5	Cranial width	rs17106852 rs6129564
Section 6	Chin protrusion	rs3827760 rs6740960 rs10238953
Section 7	Nose wing breadth	rs927833 rs17640804
Section 8	philtrum width	rs2977562
Section 9	Forehead	rs5880172
Section 10	Nose tip	rs9995821

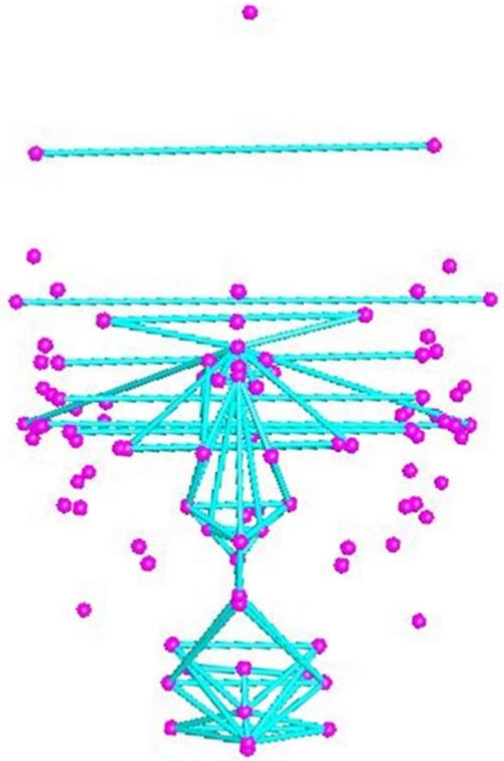

Figure 3.

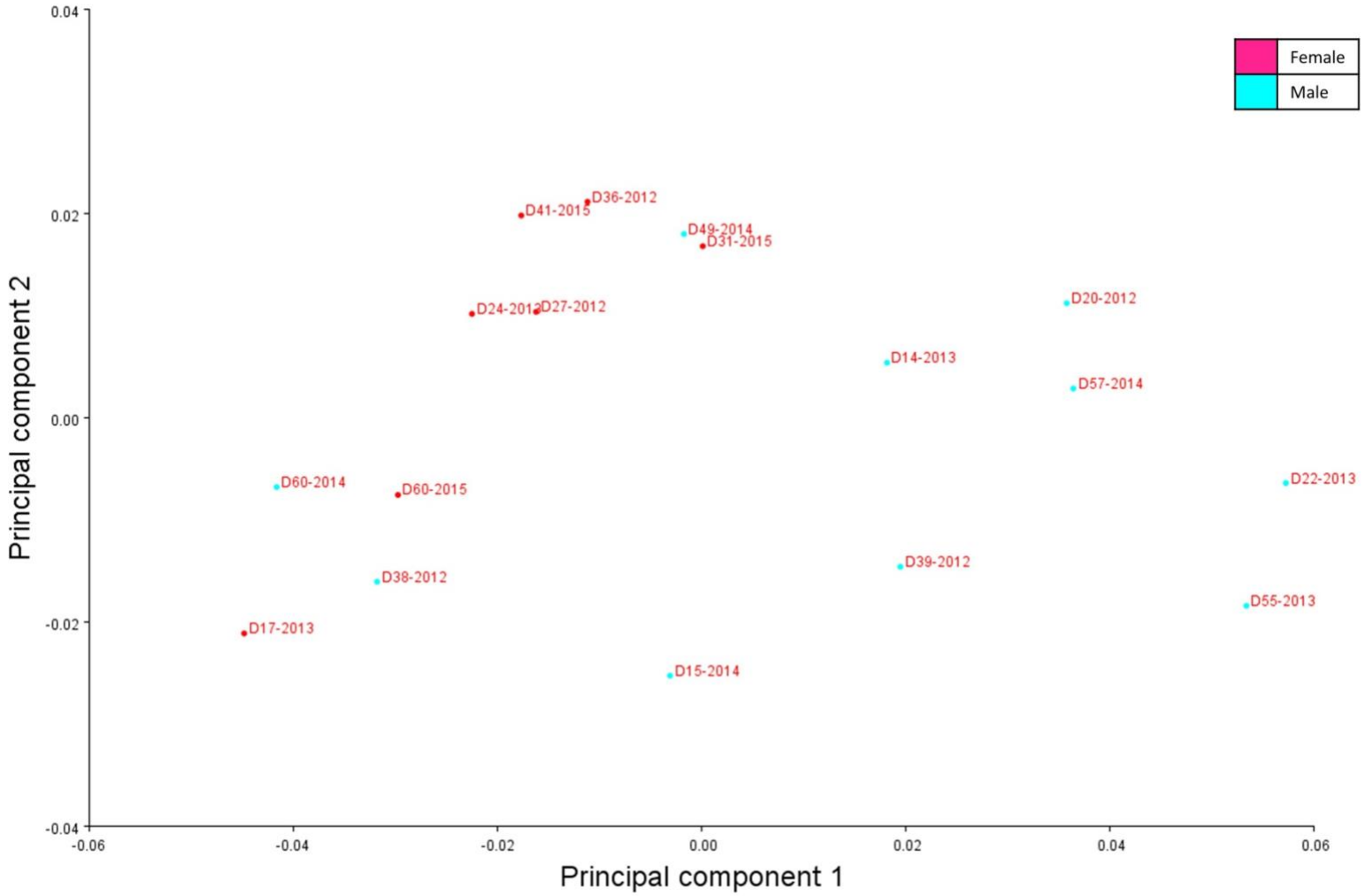

Figure 4.

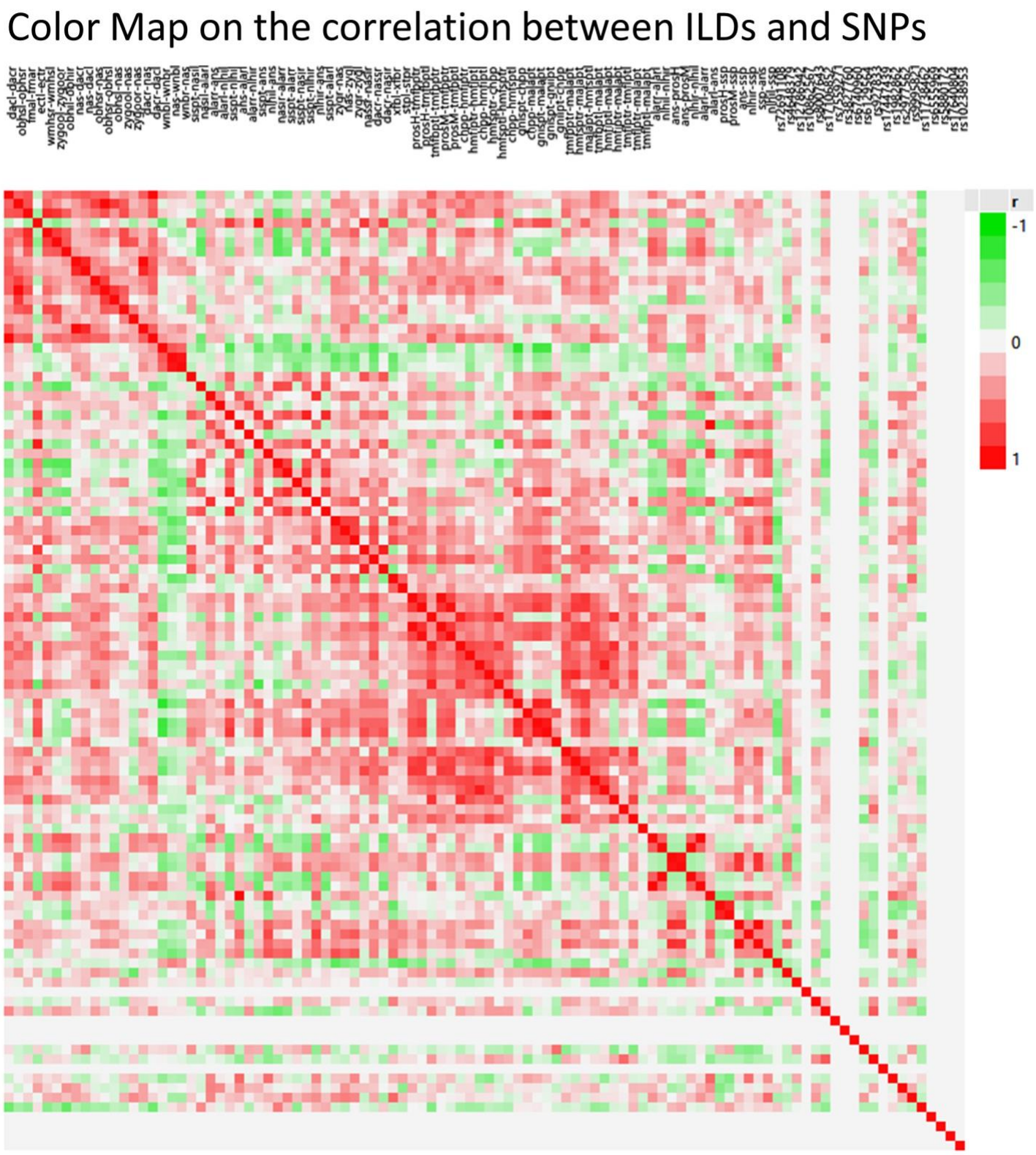

Figure 5.

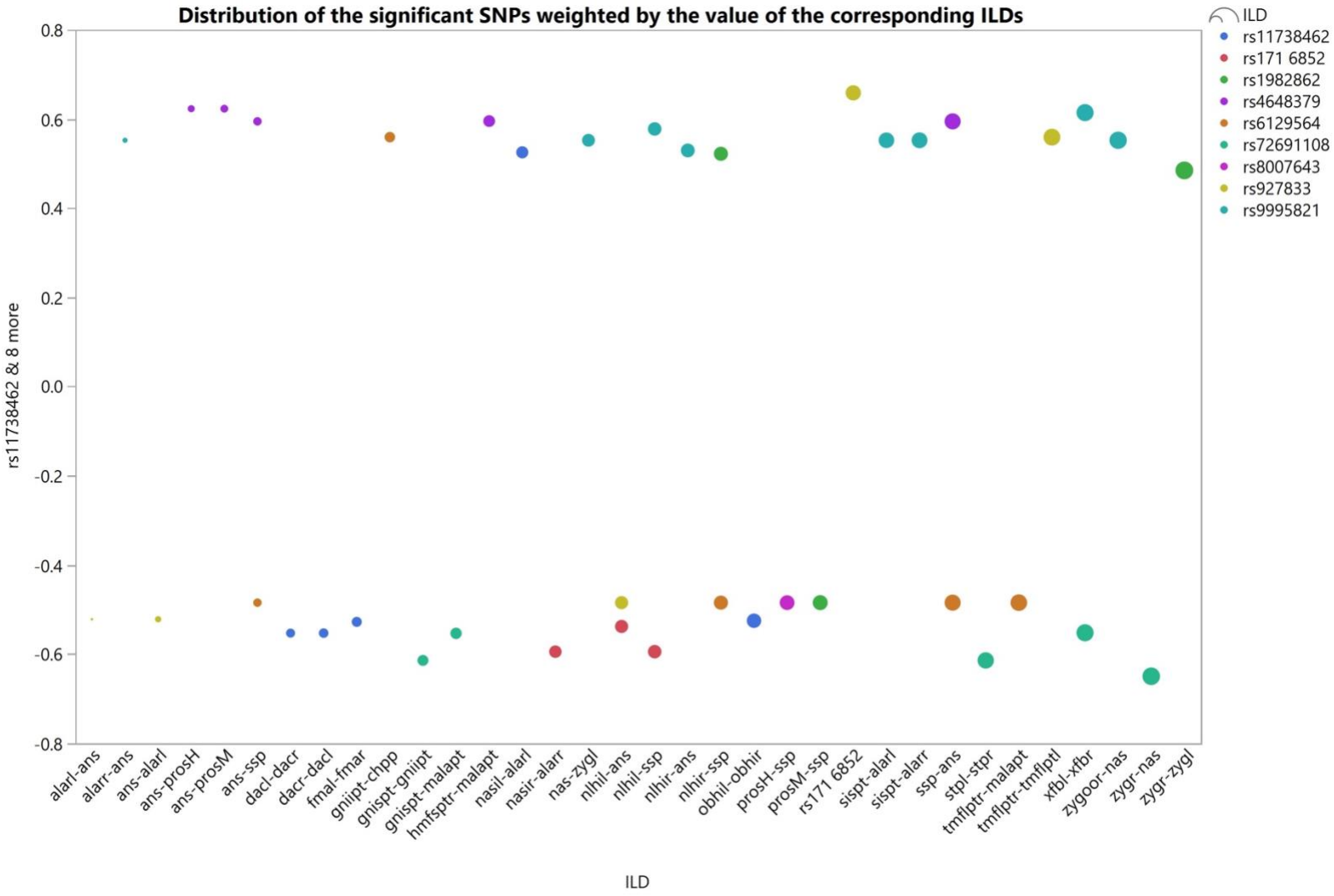
Distribution of the significant SNPs weighted by the value of the corresponding ILDs
rs11738462 & 8 more
0.8
0.6
0.4
0.2
0.0
-0.2
-0.4
-0.6
-0.8
alarl-ans
alarr-ans
ans-alarl
ans-prosH
ans-prosM
ans-ssp
dacl-dacr
dacr-dacl
fmal-fmar
gniipt-chpp
gnispt-gniipt
gnispt-malapt
hmfsptr-malapt
nasil-alarl
nasir-alarr
nas-zygl
nlhil-ans
nlhil-ssp
nlhir-ans
nlhir-ssp
obhil-obhir
prosH-ssp
prosM-ssp
rs171 6852
sispt-alarl
sispt-alarr
ssp-ans
stpl-stpr
tmflptr-malapt
tmflptr-tmfltl
xfbl-xfbr
zygoor-nas
zygr-nas
zygr-zygl
ILD
ILD
rs11738462
rs171 6852
rs1982862
rs4648379
rs6129564
rs72691108
rs8007643
rs927833
rs9995821

Figure 6.

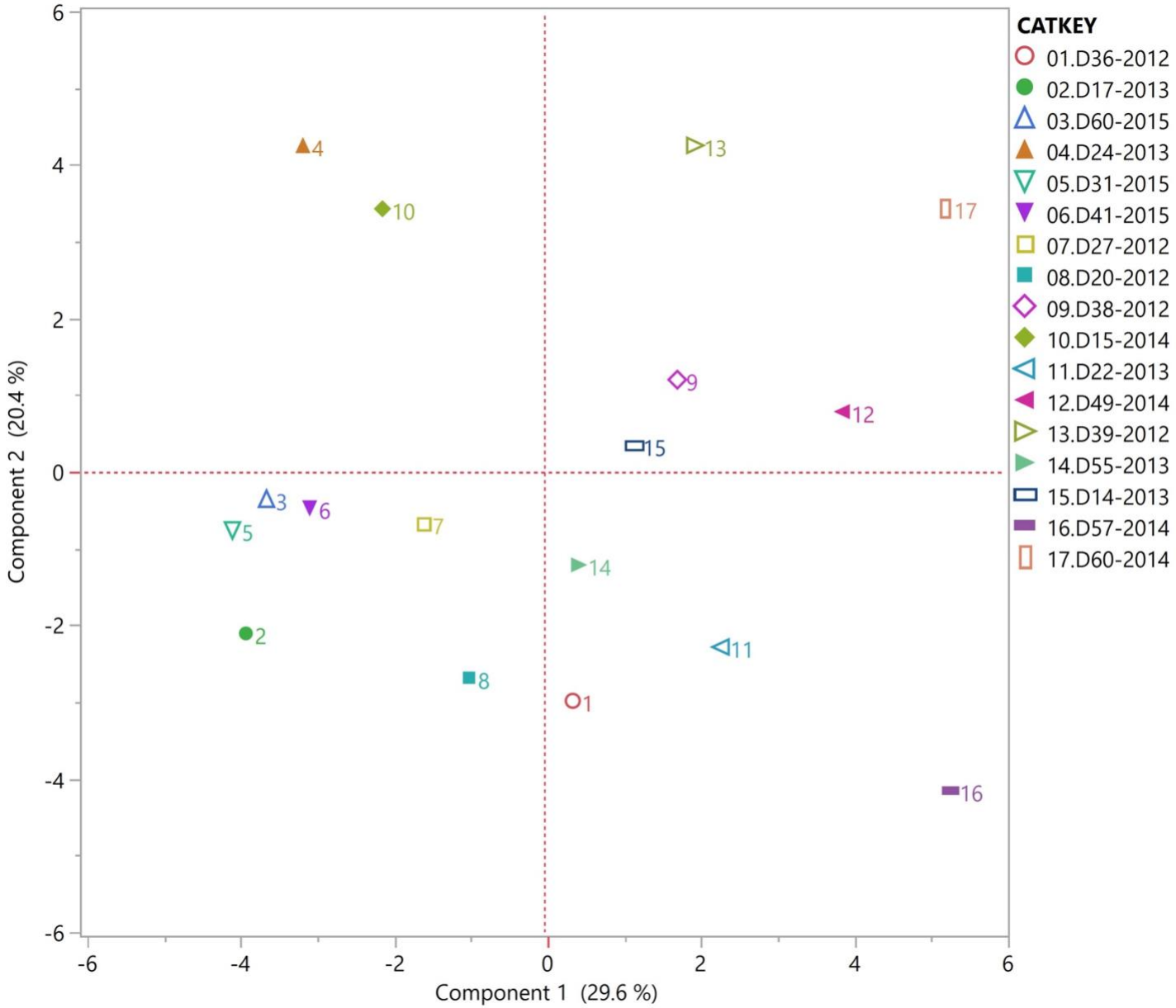
Component 2 (20.4 %)
Component 1 (29.6 %)
6
4
2
0
-2
-4
-6
CATKEY
01.D36-2012
02.D17-2013
03.D60-2015
04.D24-2013
05.D31-2015
06.D41-2015
07.D27-2012
08.D20-2012
09.D38-2012
10.D15-2014
11.D22-2013
12.D49-2014
13.D39-2012
14.D55-2013
15.D14-2013
16.D57-2014
17.D60-2014

Figure 7.

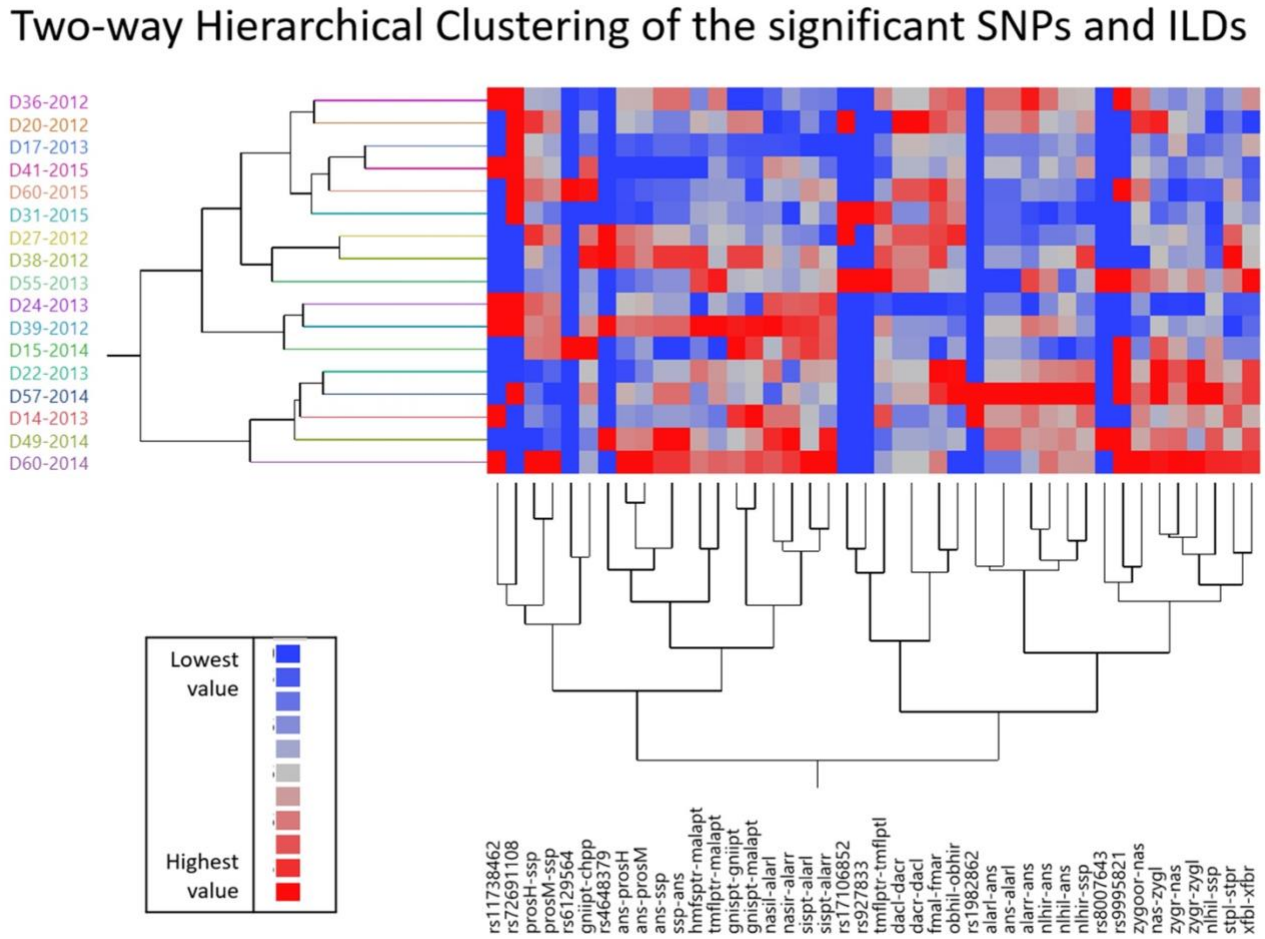
Two-way Hierarchical Clustering of the significant SNPs and ILDs
D36-2012
D20-2012
D17-2013
D41-2015
D60-2015
D31-2015
D27-2012
D38-2012
D55-2013
D24-2013
D39-2012
D15-2014
D22-2013
D57-2014
D14-2013
D49-2014
D60-2014
Lowest value
Highest value
rs11738462
rs72691108
prosH-ssp
prosM-ssp
rs6129564
gniipt-chpp
rs4648379
ans-prosH
ans-prosM
ans-ssp
ssp-ans
hmfsptr-malapt
tmfiptr-malapt
gnispt-gniipt
gnispt-malapt
nasil-alarl
nasir-alarr
sispt-alarl
sispt-alarr
rs17106852
rs927833
tmfiptr-tmfiptl
dacl-dacr
dacr-dacl
fmal-fmar
obhil-obhir
rs1982862
alarl-ans
ans-alarl
alarr-ans
nlhir-ans
nlhil-ans
nlhir-ssp
rs8007643
rs9995821
zygoor-nas
nas-zygl
zygr-nas
zygr-zygl
nlhil-ssp
stpl-stpr
xfbl-xfbr

Figure 8.

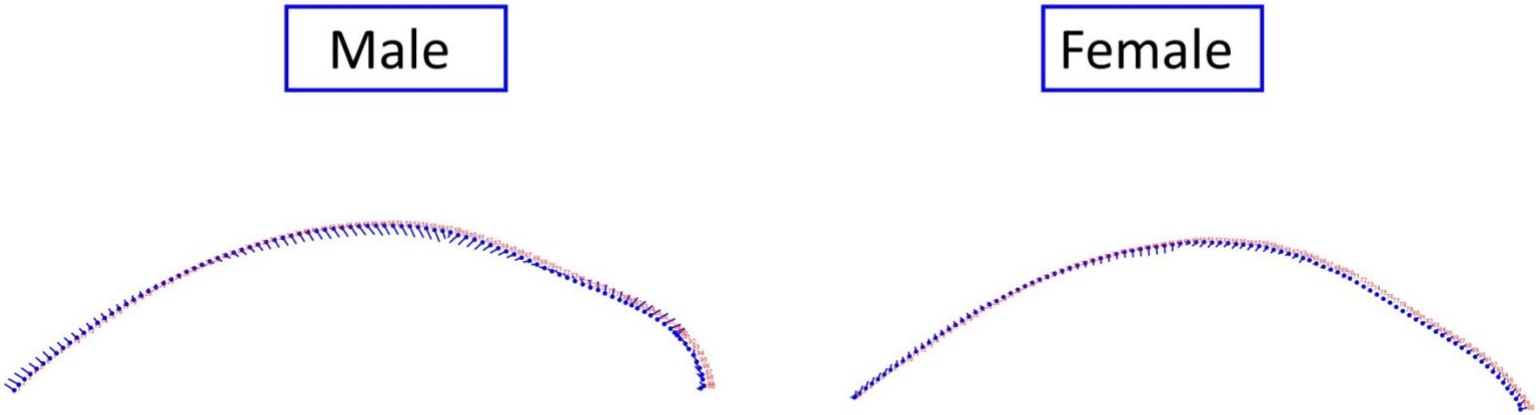

Procrustes sums of squares:	0.03
Tangent sums of squares:	0.03

Figure 9.